

# The effect of climate change on the simulated streamflow of six Canadian rivers based on the CanRCM4 regional climate model

Vivek. K. Arora<sup>1</sup>, Aranildo Lima<sup>1</sup>, Rajesh Shrestha<sup>2</sup>

<sup>1</sup>Canadian Centre for Climate Modelling and Analysis, Climate Research Division, Environment Canada, Victoria, BC, Canada

<sup>2</sup>Climate Research Division, Environment and Climate Change Canada, Victoria, BC, Canada

1

2 *Correspondence to:* Vivek K. Arora (vivek.arora@ec.gc.ca)

3 **Abstract**

4

5 The effect of climate change on the hydro-climatology, in particular streamflow, of six major  
6 Canadian rivers (Mackenzie, Yukon, Columbia, Fraser, Nelson, and St. Lawrence) is investigated  
7 by analyzing results from the historical and future simulations (RCP 4.5 and 8.5 scenarios)  
8 performed with the Canadian regional climate model (CanRCM4). Streamflow is obtained by  
9 routing runoff using river networks at 0.5° resolution. Of these six rivers, Nelson and St. Lawrence  
10 are the most regulated. As a result, the streamflow at the mouth of these rivers shows very little  
11 seasonality. Additionally, the Great Lakes significantly dampen the seasonality of streamflow for  
12 the St. Lawrence River. Mean annual precipitation (P), evaporation (E), runoff (R), and  
13 temperature increase for all six river basins in both future scenarios considered here, and the  
14 increases are higher for the more fossil fuel-intensive RCP 8.5 scenario. The only exception is the  
15 Nelson River basin for which the simulated runoff increases are extremely small. The hydrological  
16 response of these rivers to climate warming is characterized by their existing climate states. The  
17 northerly Mackenzie and Yukon River basins show a decrease in evaporation ratio (E/P) and an  
18 increase in runoff ratio (R/P) since the increase in precipitation is more than enough to offset the  
19 increase in evaporation associated with increasing temperature. For the southerly Fraser and  
20 Columbia River basins, the E/P ratio increases despite an increase in precipitation, and the R/P  
21 ratio decreases due to an already milder climate in the Pacific north-western region. The  
22 seasonality of simulated monthly streamflow is also more affected for the southerly Fraser and  
23 Columbia Rivers than for the northerly Mackenzie and Yukon Rivers as snow amounts decrease  
24 and snowmelt occurs earlier. The streamflow seasonality for the Mackenzie and Yukon rivers is  
25 still dominated by snowmelt at the end of the century even in the RCP 8.5 scenario. The simulated  
26 streamflow regime for the Fraser and Columbia Rivers shifts from a snow-dominated to a  
27 hybrid/rainfall-dominated regime towards the end of this century in the RCP 8.5 scenario. While  
28 we expect the climate change signal from CanRCM4 to be higher than other climate models,  
29 owing to the higher-than-average climate sensitivity of its parent global climate model, the  
30 results presented here provide a consistent overview of hydrological changes across six major  
31 Canadian river basins in response to a warmer climate.

32

## 33 1. Introduction

34 As the global population and the standard of living increases so does the strain on  
35 freshwater resources. The natural availability of water is determined by the balance between  
36 precipitation (P) and evaporation (E) (this includes both evaporation and transpiration from  
37 plants). When precipitation exceeds evaporation, which is determined primarily by available  
38 energy, the water that does not evaporate or transpire (either at the surface or after infiltration  
39 into the soil) termed runoff (R) is carried by the rivers to the oceans. The seasonality of  
40 precipitation, its partitioning into snow and rainfall, and the seasonality of snowmelt and  
41 evaporation, all of which are determined by the climate in a given catchment or river basin  
42 eventually determine the seasonality of runoff. As anthropogenic climate change progresses,  
43 changes in the mean annual amounts and the seasonality of these different water budget  
44 components will lead to corresponding changes in runoff (Trenberth et al., 2007). Changes in  
45 precipitation extremes are also expected to lead to corresponding changes in the extremes of  
46 streamflow. The changes in streamflow have implications for floods and power generation. While  
47 runoff is expressed in similar units to precipitation and evaporation (depth of water per unit time,  
48 e.g. mm/s or m/year), streamflow is the volume of water generated per unit time (e.g. m<sup>3</sup>/s or  
49 km<sup>3</sup>/year) and requires multiplication with the area over which runoff is generated. Streamflow  
50 is also routed down the river network which introduces a time lag and attenuation of the peak  
51 runoff.

52 Output from climate and Earth system models (ESMs) remains the primary source of  
53 information for evaluating climate change impacts. Current approaches that rely on information  
54 generated by ESMs, to obtain an estimate of how future streamflow may potentially change, may

55 be classified into two broad categories. The first approach uses simulated runoff directly from  
56 the land surface component of single or multiple climate models which may be routed  
57 downstream to obtain streamflow at the mouths of river basins and at different points along a  
58 given river network (Arora and Boer, 2001; Miller and Russell, 1992; Zhang et al., 2014). Using  
59 direct runoff output from climate models has the benefit that the calculated changes in runoff  
60 are physically consistent with the altered radiative balance of the Earth in response to increases  
61 in the concentrations of greenhouse gases (GHGs). The corresponding changes in the general  
62 circulation of the atmosphere result in the associated changes in near-surface temperature,  
63 precipitation, and the hydrological cycle. However, this approach suffers from three limitations  
64 – 1) the biases in the climate simulated by the climate model, 2) the fact that the land surface  
65 components of climate models are not calibrated for a given river basin but rather designed to  
66 operate in a reasonably realistic way over the whole globe, and 3) the coarse resolution of global  
67 climate models (GCMs). The last limitation is partially addressed when data from finer-resolution  
68 regional climate models is used. The biases in the simulated climate do affect the simulated  
69 runoff for the current climate. Despite this, the approach can effectively capture the effects of  
70 climate change including increased evaporative demand (Winter and Eltahir, 2012), reduced  
71 snowpack (Salathé et al., 2010; Shrestha et al., 2021a), increased winter streamflow, and earlier  
72 snowmelt-driven peak flow (L. Sushama et al., 2006; Poitras et al., 2011). The second approach  
73 attempts to overcome these limitations by downscaling and/or bias-correcting climate from  
74 climate models for future scenarios and uses that to drive a well-calibrated hydrological model  
75 for given catchments or river basins (Gosling et al., 2011; Ismail et al., 2020; Miller et al., 2021;  
76 Yoosefdoost et al., 2022). The second approach is more prevalent for watershed to regional scale

77 impacts and adaptation studies. Given the large effort involved in downscaling and bias-  
78 correcting raw climate data from climate models, most current impact studies use downscaled  
79 and bias-corrected data put together by other groups rather than specifically doing this for their  
80 project. Recent examples include the downscaled and bias-corrected climate data for the  
81 conterminous United States (Thrasher et al., 2013) based on climate model output from the fifth  
82 phase of the Coupled Model Intercomparison Project (CMIP5), and statistically downscaled and  
83 bias-corrected data from five CMIP5 models, available at the global scale, tailored to the  
84 requirements of the Inter-Sectoral Impact Model Intercomparison Project (ISIMIP) (Lange, 2019).  
85 Both these data sets have found large applications in the impacts and adaptation community.  
86 The processes of downscaling and bias correction are distinct, and they both have their inherent  
87 limitations. There are several examples of the limited ability of bias-correction to correct and  
88 downscale variability, and that bias-correction can potentially cause implausible climate change  
89 signals (Maraun, 2016; Maraun et al., 2017). There are also uncertainties, substantial  
90 contradictions, and sensitivity to assumptions between the different downscaling methods  
91 (Hewitson et al., 2014).

92         Finally, while land surface models are typically used within the coupled framework of  
93 climate models, hydrological models are typically used as a standalone model for impact studies.  
94 While the primary output quantities from hydrological models are runoff and streamflow, land  
95 surface models output a range of water, energy, and CO<sub>2</sub> fluxes (Blyth et al., 2021; Fisher and  
96 Koven, 2020). The layer of air directly above the land surface, commonly referred to as the  
97 atmospheric or planetary boundary layer, is affected by surface-atmosphere exchanges of energy  
98 and water and extends upward into the atmosphere. A realistic representation of turbulent fluxes

99 of energy and water in the planetary boundary layer is essential to the transport of moisture and  
100 energy through the atmosphere. As a result, while calibration of hydrological models to  
101 reproduce observed streamflow is a routine exercise (Chegwidden et al., 2019; Hattermann et  
102 al., 2018; Huang et al., 2020; Hundecha et al., 2020), land surface models cannot be calibrated to  
103 reproduce a single or a small subset of quantities. This aspect of land surface versus hydrological  
104 models is also addressed briefly in Bolaños Chavarría et al. (2022). A review by Overgaard et al.  
105 (2006) also attempts to differentiate land surface models from hydrological models. In contrast  
106 to hydrological models, land surface models are expected to reproduce reasonably realistic  
107 estimates of a range of energy, water, and CO<sub>2</sub> fluxes over the whole globe. The philosophy  
108 behind land surface models, as they are used in the context of climate models, is that given 1) a  
109 model's structure and parameterizations, 2) the driving geophysical data for fields such as  
110 vegetation cover, soil depth, and soil texture, and 3) the driving meteorological variables, a model  
111 is expected to reasonably realistically reproduce various components of the water, energy, and  
112 carbon cycle at the global scale. The global scale of land surface models within the framework of  
113 climate models precludes tuning of their parameters for individual grid cells or for a region (e.g.  
114 a river basin) to reproduce a small subset of model outputs.

115 While well-calibrated hydrological models are generally suitable for a given catchment or  
116 a river basin their application cannot be easily extended to large-scale global or regional  
117 hydrologic modelling studies since it is typically not feasible to tune model parameters for all grid  
118 cells in a large domain. For a large region like Canada correctly representing anthropogenic  
119 regulation using downscaled and bias-corrected climate data from an ensemble of climate  
120 models is a challenging task. As a result, this has been done for only a few selected river basins,

121 considering only one basin at a time. In the end, both approaches have their strengths and  
122 limitations for assessing climate change impacts on hydrology and can be considered  
123 complementary to each other.

124 Future hydrologic projections using the second approach (hydrological modes driven by  
125 statistically downscaled and bias-adjusted climate models) are available for selected river basins  
126 in Canada. The results over the Prairies and British Columbia (Shrestha et al., 2021b; Sobie and  
127 Murdock, 2022) generally indicate shorter snow cover duration, earlier snowmelt, and reduced  
128 annual maximum snow water equivalent as the climate warms. Streamflow projections across  
129 Canada generally indicate earlier snowmelt-driven peak flow, increased winter flow, and  
130 decreased summer flow (Budhathoki et al., 2022; Dibike et al., 2021; Islam et al., 2019;  
131 MacDonald et al., 2018; Shrestha et al., 2019). Annual streamflow is projected to increase, with  
132 higher increases in the northern basins (Bonsal et al., 2020; Stadnyk et al., 2021). However, these  
133 projections are based on different climate and hydrological models, downscaling methods,  
134 emissions scenarios, and future periods, and no consistent set of projections is available across  
135 all major river basins of Canada.

136 In this study, we have used the first approach to provide a consistent set of projections  
137 across all major river basins of Canada, while being cognizant of its limitations. We investigate  
138 the effect of climate change on the annual, monthly, and daily streamflow characteristics of six  
139 major Canadian rivers (Mackenzie, Yukon, Columbia, Fraser, Nelson, and St. Lawrence) using  
140 runoff output from simulations performed with version 4 of the Canadian Regional Climate  
141 Model (CanRCM4) (Scinocca et al. 2016). The river basins of the Yukon and Columbia Rivers cover  
142 part of the United States of America as well. We used daily runoff generated from CanRCM4 for

143 the historical period and for the two future scenarios (representative concentration pathways  
144 (RCP) 4.5 and 8.5). The spatial resolution of runoff data from CanRCM4 is  $0.22^\circ$  which is  
145 equivalent to about 12 km at  $60^\circ$  N (Canada lies between approximately  $42^\circ$ N and  $83^\circ$ N). We  
146 then routed this runoff through river networks at  $0.5^\circ$  resolution to evaluate streamflow at the  
147 mouths of major Canadian rivers. The Mackenzie, Yukon, and Fraser Rivers are somewhat less  
148 regulated than the heavily regulated Nelson, Columbia, and St. Lawrence Rivers. The routing  
149 scheme used here does not take into account dams and reservoirs and therefore the modelled  
150 streamflow represents natural streamflow. This aspect is discussed in more detail in Section 2.

## 151 **2. Models and data**

152 Equation (1) summarizes the water balance over a given grid cell or a river basin for a  
153 given timescale.

$$154 \qquad P = E + R + \Delta S \qquad (1)$$

155 where  $\Delta S$  is the change in water storage including that in soil moisture, snow, and the canopy  
156 water storage. All terms are expressed in depth per unit time units (e.g. mm/year). When a  
157 system is in equilibrium, at annual or longer timescales  $\Delta S = 0$  and  $P = E + R$ .  $\Delta S$ , however,  
158 may not be zero even over long timescales when a system is not in equilibrium e.g., when snow  
159 is accumulating or is melting consistently. We evaluated the P, E, and R components of equation  
160 (1) simulated by CanRCM4 for each of the six river basins, considered in this analysis, and routed  
161 R to obtain streamflow at the river mouths.

162

### 163 **2.1 The Canadian Regional Climate Model (CanRCM4)**



164 CanRCM4 uses the fourth-generation Canadian atmospheric physics (CanAM4) package  
165 (von Salzen et al., 2013), which is the product of a multi-decadal program of climate model  
166 development at the Canadian Centre for Climate Modelling and Analysis (CCCma), a section  
167 within Environment and Climate Change Canada. The CanAM4 atmospheric physics package is  
168 also used in CanESM2 (Arora et al., 2011) which contributed results to CMIP5. The difference  
169 between CanRCM4 and CanESM2, other than the former being a regional climate model and the  
170 latter being a comprehensive global ESM, is that CanRCM4 employs the limited-area  
171 configuration of the Global Environmental Multiscale (GEM) model (Côté et al., 1998), which uses  
172 a semi-Lagrangian dynamical core for advection in the atmosphere and is developed by  
173 Environment and Climate Change Canada's Recherche en Prévision Numérique (RPN) where it is  
174 used both for global and regional numerical weather prediction. CanESM2 on the other hand  
175 uses a spectral dynamical core for advection in the atmosphere. CanRCM4 is driven at its  
176 boundaries with data from its parent model (CanESM2). An overview and technical details of the  
177 coordinated global and regional climate modelling effort used to develop the CanESM2-CanRCM4  
178 system are described in detail by Scinocca et al. (2016). Results from the model's North American  
179  $0.22^\circ$  domain, for a single ensemble member, are primarily used here. In addition, we also used  
180 runoff from CanRCM4  $0.44^\circ$  resolution simulations for the North American domain because of  
181 the availability of a large ensemble (LE) of 50 members (CanRCM4 LE) (ECCC, 2018). The large  
182 ensemble simulations allow the consideration of CanRCM4's internal variability, which is an  
183 intrinsic property of the climate system and models, that is largely irreducible and could account  
184 for a large fraction of the inter-climate model spread (Deser et al., 2020). The results used here  
185 from CanRCM4 form part of its contribution to the coordinated regional climate downscaling

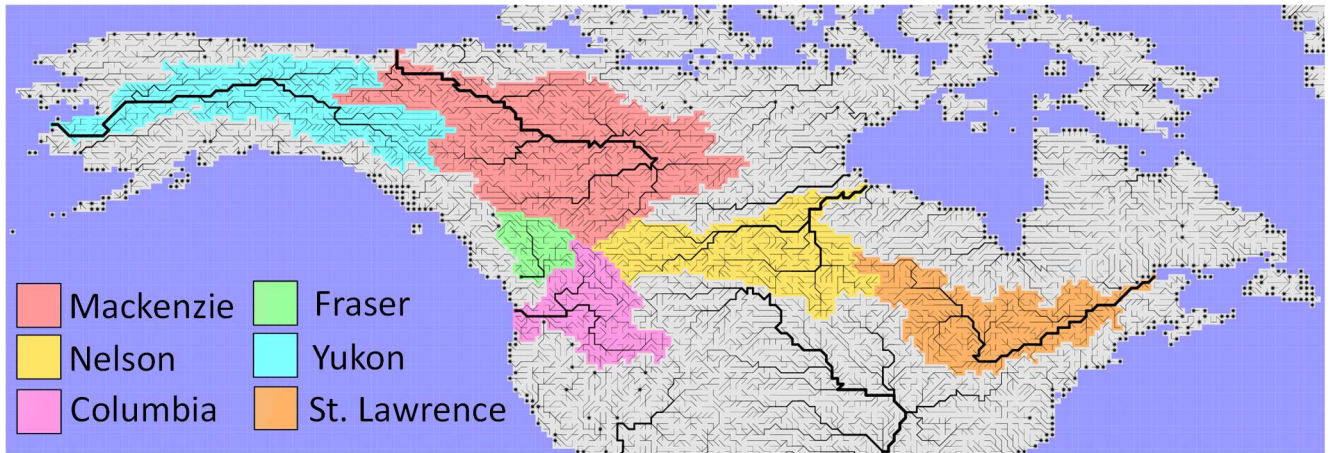
186 experiment (CORDEX) effort. The North American domain of CanRCM uses a rotated latitude-  
187 longitude projection with the North Pole at longitude  $83^{\circ}$  E and latitude  $42.5^{\circ}$  N, as opposed to  
188 the geographic North Pole (longitude  $0^{\circ}$ E, latitude  $90^{\circ}$  N).

189         The land surface component in CanAM4 is the coupled CLASS-CTEM model. The physical  
190 processes are based on the Canadian Land Surface Scheme (CLASS) (Verseghy, 1991; Verseghy et  
191 al., 1993), and biogeochemical processes (which simulate vegetation as a dynamic component of  
192 the climate system) are based on the Canadian Terrestrial Ecosystem Model (CTEM) (Arora and  
193 Boer, 2003, 2005). The configuration of CLASS-CTEM used in CanESM2 and CanRCM4 uses three  
194 soil layers with thicknesses of 0.10, 0.25, and 3.75 m. Liquid and frozen soil moisture contents,  
195 and soil temperature, are determined prognostically for the three soil layers. The temperature,  
196 albedo, mass, and density of a single-layer snow pack (when environmental conditions permit  
197 snow to exist) are also prognostically modelled. Surface runoff is generated in CLASS when  
198 precipitation intensity exceeds infiltration capacity and when the top soil layer is saturated. The  
199 rainwater and snow melt that infiltrate the soil are available for soil evaporation and  
200 transpiration. Any remaining water percolates down the soil profile and comes out at the bottom  
201 of the soil profile and is termed drainage. Combined surface runoff and drainage constitute total  
202 runoff. Like most land surface components of ESMs, CLASS does not include a groundwater  
203 representation. Surface runoff and drainage from CLASS are used as input into a large-scale river  
204 routing scheme to route runoff and obtain streamflow at the mouth of the rivers considered in  
205 this study as explained in the next section.

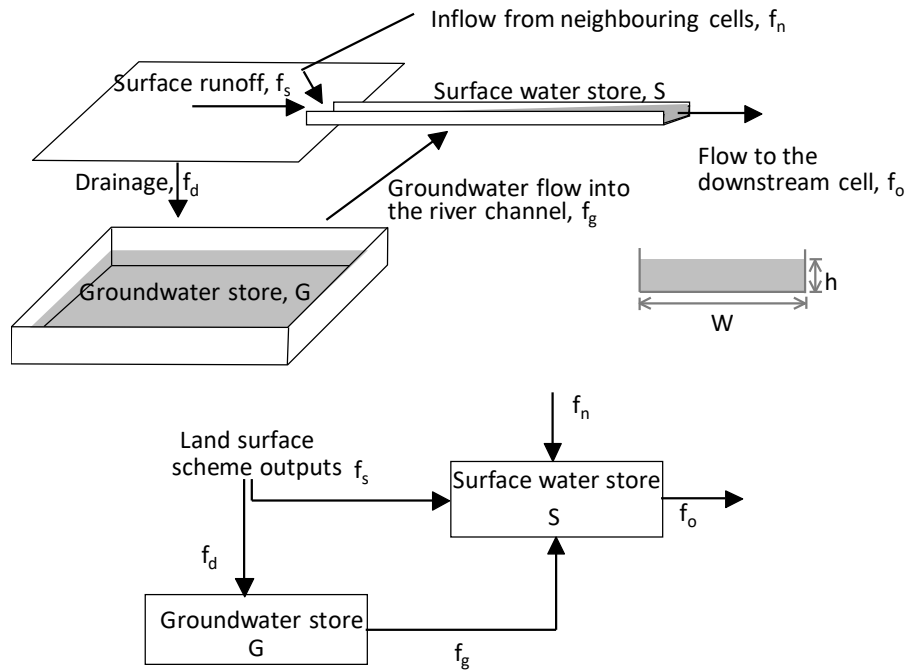
## 206 **2.2 Variable velocity routing model**

207           The variable velocity river routing scheme of Arora and Boer (1999) that is implemented  
208 in the family of Canadian ESMs (CanESMs) (Arora et al., 2009, 2011; Swart et al., 2019) is used to  
209 route daily runoff from CanRCM4. This routing scheme has been implemented in various versions  
210 of CanESMs at a spatial resolution of  $2.81^\circ$  since the year 2000. For this study, the routing scheme  
211 was implemented at a spatial resolution of  $0.5^\circ$ . The reason for using river routing at  $0.5^\circ$   
212 resolution instead of scaling river networks to the  $0.22^\circ$  rotated latitude-longitude projection of  
213 CanRCM4 's North American domain is that scaling river networks is a non-trivial and  
214 cumbersome task that cannot be fully automated (Arora and Harrison, 2007). In contrast,  
215 conservatively regridding runoff from one spatial resolution to another is a straightforward  
216 process. In addition, it has been shown that routing is not very sensitive to the spatial scale at  
217 which it is performed. Specifically, Arora et al. (2001) evaluated the Arora and Boer (1999) routing  
218 scheme together with the WATROUTE routing scheme at  $\sim 350$  km and  $\sim 25$  km spatial resolutions,  
219 respectively, for the Mackenzie River basin. The two routing schemes were driven with the same  
220 runoff. Arora et al. (2001) conclude that for the purpose of realistically modelling streamflow at  
221 the mouth of the rivers in climate models, flow routing at large spatial scales gives similar results  
222 to routing at finer spatial scales. In our study, the difference between the spatial resolution of  
223 runoff ( $0.22^\circ$  and  $0.44^\circ$ ) from the CanRCM4 model and routing ( $0.5^\circ$ ) is much smaller than the  
224 Arora et al. (2001) study. As a result, we do not expect that routing at a slightly different spatial  
225 resolution than runoff will lead to significant differences in the simulated streamflow. The routing  
226 scheme needs river flow directions and these are obtained from the Total Integrating Runoff  
227 Pathways (TRIP) data set (<http://hydro.iis.u-tokyo.ac.jp/~taikan/TRIPDATA/TRIPDATA.html>, last  
228 accessed July 2023) of Oki and Sud (1998). The TRIP data are available at the regular latitude-

229 longitude grid with the geographic North Pole at its usual location ( $0^{\circ}$  E,  $90^{\circ}$  N). Figure 1 shows  
230 the river networks at  $0.5^{\circ}$  resolution based on TRIP data which also identifies the six river basins  
231 investigated in this study. The Fraser River (identified by the light green colour) appears to have  
232 a river mouth over land. This is because the Fraser River drains into the narrow Strait of Georgia  
233 which is not resolved at the  $0.5^{\circ}$  resolution of the TRIP data set. In addition, the TRIP data set  
234 does not resolve any inland lakes and provides river flow directions over grid cells that are lakes.  
235 This is in fact helpful because it avoids discontinuities in the river network.



236  
 237 **Figure 1:** River flow networks at 0.5° resolution used in this study. The major river basins for  
 238 which streamflow and runoff are analyzed in this study are also identified.



239  
 240  
 241 **Figure 2:** Schematic of the Arora and Boer (1999) river routing scheme used in this study to route  
 242 runoff simulated by CanRCM4.

243  
 244 Figure 2 shows the schematic of the routing scheme which uses surface runoff and  
 245 drainage outputs from the land surface scheme. The variable velocity routing scheme used here

246 is described briefly below and more details can be found in Arora and Boer (1999). The water  
 247 balance within a grid cell for its surface  $S$  ( $m^3$ ) and groundwater  $G$  ( $m^3$ ) stores is given by

$$248 \quad \frac{dS}{dt} = f_s + f_n + f_g - f_o \quad (2)$$

$$249 \quad \frac{dG}{dt} = f_d - f_g \quad (3)$$

250 where,  $f_s$  and  $f_d$  are the surface runoff and drainage (or baseflow) estimates given by the land  
 251 surface scheme,  $f_n$  and  $f_o$  are the surface water inflow from the adjacent upstream neighbouring  
 252 grid cell(s) and outflow to the downstream grid cell respectively, and  $f_g$  is the groundwater  
 253 outflow from the groundwater reservoir to the surface water reservoir within a grid cell as shown  
 254 in Figure 2. The fluxes are represented in  $m^3/s$ .

255 A river channel is assumed to be rectangular and the width ( $W$ ) of the river at every point  
 256 along the river network is specified a priori. This river width in meters is calculated based on its  
 257 geomorphological relationship with mean annual discharge. The surface runoff contributes  
 258 directly to the surface water store which is essentially the amount of water in the rectangular  
 259 river channel between two grid cells. The flow velocity ( $V$ ,  $m/s$ ) is calculated using the Mannings  
 260 formula (Manning, 1891).

$$261 \quad V = \frac{1}{r} R^{2/3} S^{1/2} = \frac{1}{r} \left( \frac{A}{P} \right)^{2/3} n^{1/2} = \frac{1}{r} \left( \frac{Wh}{W+2h} \right)^{2/3} n^{1/2} \quad (4)$$

262 where  $r$  is the unitless Mannings roughness coefficient (a default value of 0.04 is used),  $A$  is the  
 263 area of the river channel ( $m^2$ ),  $P$  is the wetted perimeter (m), and  $h$  is the depth of water in the  
 264 channel (m). The slope  $n$  (unitless) of the channel is calculated using elevation difference and the  
 265 river length between two grid cells.

266 The river channel storage  $S$  is assumed to be a linear function of outflow discharge, so

267 
$$S = \tau f_o = \frac{L}{V} AV = LA = LWh \quad (5)$$

268 where  $\tau$  is the travel time between the grid cell under consideration and its downstream  
269 neighbor given by  $\tau = L/V$ , where  $L$  is the distance between the grid cells (m). The outflow  $f_o$  is  
270 given by

271 
$$f_o = AV = WhV = Wh \frac{1}{r} \left( \frac{Wh}{W+2h} \right)^{2/3} n^{1/2} \quad (6)$$

272 and substituting (5) and (6) into (2) yields

273 
$$\frac{dh}{dt} = \frac{1}{LW} \left( I - \frac{W^{5/3} h^{5/3}}{r(W+2h)^{2/3}} n^{1/2} \right) \quad (7)$$

274 where  $I$  ( $m^3/s$ ) is the total inflow into a grid cell ( $I = f_s + f_n + f_g$ ). Equation (7) describes the flow in  
275 terms of the rate of change of flow depth for a given river section. An explicit forward step finite  
276 difference approximation for (7) yields

277 
$$h(t + 1) = h(t) + \frac{\Delta t}{LW} \left( I(t) - \frac{W^{5/3} h(t)^{5/3}}{r(W+2h(t))^{2/3}} n^{1/2} \right) \quad (8)$$

278 Flow velocity and outflow discharge for the river channel at any time step can be obtained using  
279 equations (4) and (6). For the  $0.5^\circ$  resolution used here, a stable solution of (8) is obtained with  
280  $\Delta t$  equal to around 10 minutes. The approach yields dynamically-varying flow depth, velocity,  
281 and discharge through the river channel in response to changing surface and baseflow runoff  
282 inputs from the land surface model.

283 The groundwater component of the routing model assumes that groundwater storage,  $G$ ,  
284 is a linear function of groundwater outflow,  $f_g$ .

$$285 \quad G = \tau_g f_g \quad (9)$$

286 The delay in groundwater storage ( $\tau_g$ ) is based on the dominant soil texture type and is set to 10,  
287 35, and 65 days if the dominant soil type in each grid cell is sand, silt, and clay, respectively,  
288 following Arora and Boer (1999). Substituting  $G$  in equation (3) yields

$$289 \quad \tau_g \frac{df_g}{dt} = f_d - f_g \quad (10)$$

290 and following Arora and Boer (1999) we use the following expression

$$291 \quad f_g(t + 1) = f_g(t) e^{-\Delta t/\tau_g} + \left(1 - e^{-\frac{\Delta t}{\tau_g}}\right) f_d(t) \quad (11)$$

292 to determine discharge from the groundwater reservoir within a grid cell and to step forward in  
293 time, where a time step  $\Delta t$  equal to three hours is used. The simplistic form of equation (11)  
294 allows to use a much larger time step than the time step of 10 minutes required for equation (8).

295 The routing scheme used here does not consider the flow regulation effect of dams and  
296 reservoirs. It, however, does consider the effect of lakes and ice jams in a simple manner. The  
297 global lake data set from Kourzeneva et al. (2012) is used which prescribes the fractional coverage  
298 of sub-grid lakes and the five Laurentian Great Lakes (Lakes Superior, Michigan, Huron, Ontario,  
299 and Erie). In particular, the flow at the mouth of the St. Lawrence River is affected significantly  
300 by the Great Lakes. The hydraulic residence time of water in the Great Lakes varies from about 2  
301 years for Lake Erie to about 200 years for Lake Superior (Quinn, 1992). As a result, even in the



302 absence of anthropogenic flow regulation for the St. Lawrence River, we expect the streamflow  
303 at its mouth to show very little seasonality compared to the usual spring peak of Canadian rivers  
304 dominated by snowmelt. The simple approach used here delays the streamflow flowing into a  
305 grid cell with a lake fraction greater than 60% using an e-folding time scale of 300 days similar to  
306 the treatment of the groundwater reservoir (Figure 2) (Arora and Boer, 1999). For the St.  
307 Lawrence River, the effect of delay caused by the Great Lakes is much larger than that of the  
308 anthropogenic flow regulation.

309           Ice jams and breakups are complex thermal and mechanical events and therefore  
310 challenging to model. They occur on all Canadian rivers with varying degrees and depend on  
311 winter temperatures, the river bathymetry, and the physical and geomorphological conditions of  
312 rivers (Beltaos, 2000; Prowse, 1986). The winter freezing of river water inevitably leads to a slow  
313 down of river flow velocity. When water cannot move downstream, upstream flooding results.  
314 Here, we have used a simple approach that increases Manning's roughness coefficient for the  
315 Mackenzie and the Yukon Rivers (which are the most northerly and therefore affected the most  
316 by ice jams) for the period January to June. The value of Manning's roughness coefficient is  
317 increased linearly from 0.04 to 0.08 from 1 January to 31 January, kept at 0.08 from 1 Feb to 31  
318 May, and then reduced linearly from 0.08 to 0.04 over the period June 1 to 30 June. Chen and  
319 She (2020) report the trend in river ice breakup dates for the Mackenzie and Yukon Rivers to be  
320 around -0.3 and -1.3 days/decade for the 1950-2016 period, where the negative sign indicates  
321 that the ice breakup is occurring earlier. Assuming the same trend, the breakup dates would  
322 occur about 2.5 and 11 days earlier towards the end of this century, respectively, for the  
323 Mackenzie and Yukon rivers. This simple approach reduces the river flow velocity during the

324 months that are most affected by river ice jams. Although this is not a perfect nor a complete  
325 approach this simple treatment allows to improve the streamflow seasonality for the Mackenzie  
326 and Yukon rivers. For the southerly Fraser and Columbia rivers such treatment was not necessary.  
327 Consideration of a higher roughness coefficient for the St. Lawrence River to account for ice jams  
328 does not affect its streamflow's seasonality (or rather the lack of it) which is overwhelmingly  
329 determined by the delay and storage caused by the Great Lakes.

### 330 **2.3 Modelled and observation-based data**

331 The CMIP5 historical simulation covers the period 1850-2005 and the future scenarios  
332 cover the period 2006-2100. We used daily runoff from CanRCM4 from its 0.22° North American  
333 domain for the 20 years 1986-2005 from one ensemble member of the historical simulation and  
334 for the 20 years 2081-2100 from one ensemble member each for the two future scenarios (RCP  
335 4.5 and RCP 8.5, Moss et al. (2010)). The RCP 8.5 is the highest baseline emissions scenario where  
336 future development is based on continuous fossil-fuel development. As a result, CO<sub>2</sub> emissions  
337 and concentrations increase throughout the 21<sup>st</sup> century and CO<sub>2</sub> concentration in the year 2100  
338 is around 1100 ppm. RCP 4.5 is a moderate emissions scenario in which emissions peak around  
339 2040 and then decline: as a result CO<sub>2</sub> somewhat stabilizes to around 550 ppm by the year 2100.  
340 Since the CanRCM4 data are available on a rotated latitude-longitude grid and the river routing  
341 is performed on a regular latitude-longitude grid (following the TRIP data), the runoff data from  
342 CanRCM4 are conservatively regridded to the global 0.5° grid using climate data operators (CDO)  
343 (<https://code.mpimet.mpg.de/projects/cdo/embedded/index.html#x1-7170002.12.5>, last  
344 accessed Dec 2023) as mentioned earlier. These runoff data are then used as input into the  
345 routing model. The 20-year runoff data (1986-2005 for the historical simulation, and 2081-2100

346 for the future scenarios) are concatenated into a 40-year time series for each simulation  
347 (historical, RCP 4.5, and RCP 8.5). These data are then input into the routing model and the last  
348 20 years of simulated streamflow are analyzed. The 20-year spin-up is sufficient to allow the  
349 surface and groundwater stores to fill up and reach equilibrium. The simulated precipitation and  
350 temperature from CanRCM4 are compared against observation-based data from the CRU TS 4.07  
351 product (Harris et al., 2020).

352 The simulated streamflow is compared against observation-based estimates obtained  
353 from the Global Runoff Data Centre (GRDC) for the stations that are closest to the river mouths.  
354 Table 1 lists the drainage areas of all rivers considered in this study as discretized in the TRIP data  
355 set and at the stations closest to the river mouth. For the Columbia River, which is heavily  
356 regulated, we obtain an estimate of the naturalized flow with no regulation and no irrigation  
357 provided by the Bonville Power Administration (BPA) for the station VAN (near Vancouver,  
358 Washington, USA) ([https://www.bpa.gov/energy-and-services/power/historical-streamflow-](https://www.bpa.gov/energy-and-services/power/historical-streamflow-data)  
359 [data;https://www.bpa.gov/-/media/Aep/power/historical-streamflow-reports/historic-](https://www.bpa.gov/-/media/Aep/power/historical-streamflow-reports/historic-streamflow-nrni-flows-1929-2008-corrected-04-2017.csv)  
360 [streamflow-nrni-flows-1929-2008-corrected-04-2017.csv](https://www.bpa.gov/-/media/Aep/power/historical-streamflow-reports/historic-streamflow-nrni-flows-1929-2008-corrected-04-2017.csv), last accessed July 2023). The drainage  
361 area of the Columbia River upstream of the VAN station is 616960 km<sup>2</sup> and does not include  
362 discharge contributions from three tributaries (Willamette, Cowlitz, and Lewis Rivers). Of these  
363 three tributaries, the contribution from Willamette is the largest. We obtained naturalized  
364 streamflow for the Willamette River at the station SVN (drainage area 25,600 km<sup>2</sup>) also from  
365 BPA's website ([https://www.bpa.gov/-/media/Aep/power/historical-streamflow-](https://www.bpa.gov/-/media/Aep/power/historical-streamflow-reports/correction-20220801.zip)  
366 [reports/correction-20220801.zip](https://www.bpa.gov/-/media/Aep/power/historical-streamflow-reports/correction-20220801.zip), from the file SVN6ARF\_daily\_COR.xlsx) and added it to the  
367 naturalized streamflow at the station VAN. This yields naturalized streamflow for the entire

368 Columbia River basin, except the smaller Cowlitz, and Lewis Rivers, and represents a drainage  
 369 area of 642,560 km<sup>2</sup> (see Table 1).

370 The Nelson River is affected by two large lakes, Lake Winnipeg and Lake Manitoba, and it  
 371 is also heavily regulated. It currently has five dams towards the end of its journey as it flows into  
 372 Hudson Bay. There are no upstream gauging stations close to the first upstream dam. In addition,  
 373 water is also diverted from Churchill to the Nelson River. We were unable to obtain naturalized  
 374 flow for the Nelson River from the Manitoba hydroelectricity company. Due to anthropogenic  
 375 flow regulation on the Nelson River, the present-day streamflow shows very little seasonality (as  
 376 shown later). As a result, we do not evaluate the simulated daily or monthly streamflow for the  
 377 Nelson River and focus only on its mean annual value.

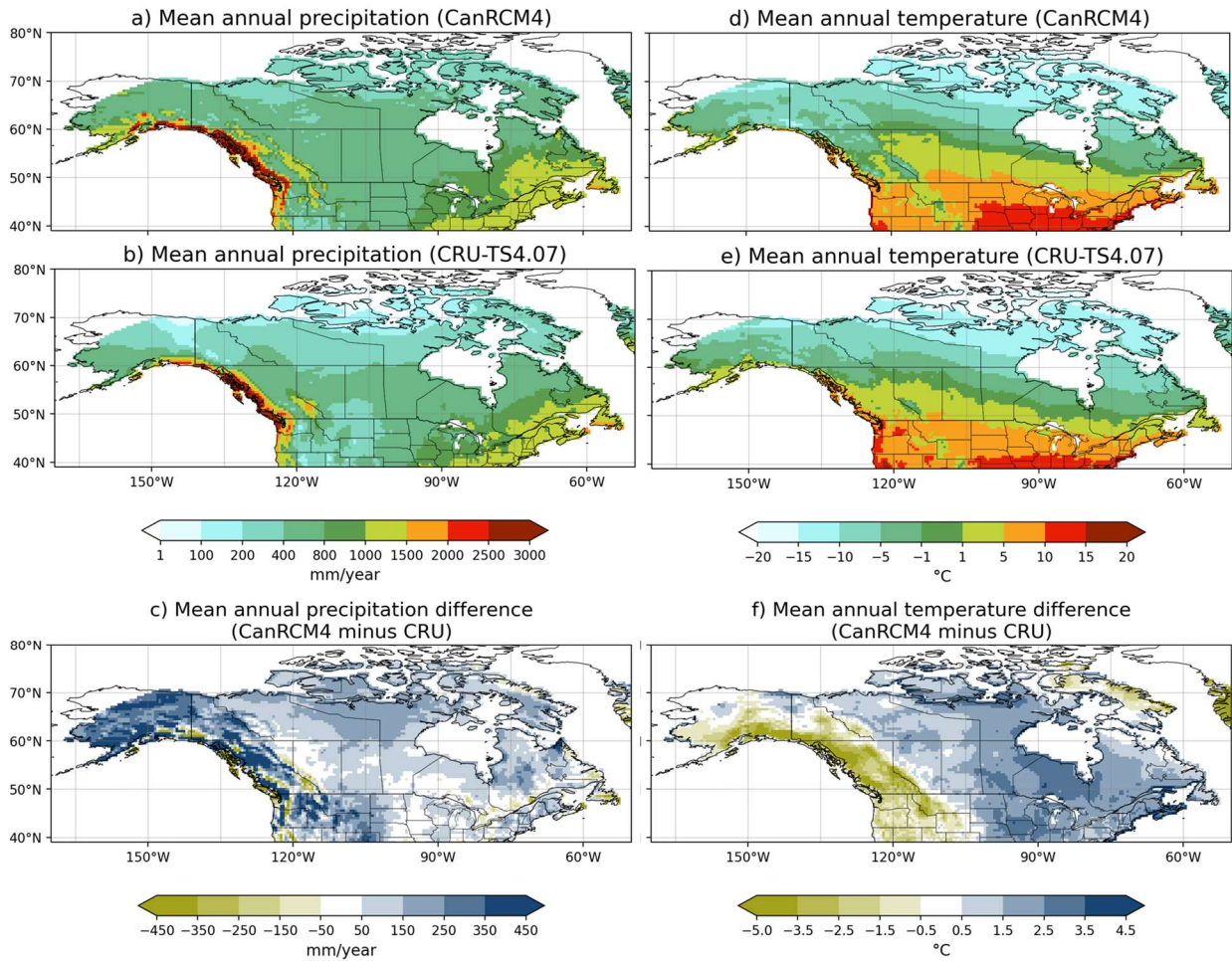
378 **Table 1:** Comparison of river basin areas as represented in the TRIP data and at the gauging  
 379 station closest to the river mouth for the river basins considered in this study as obtained from  
 380 the GRDC.

381

River basin	River basin area (million km <sup>2</sup> )		Gauging station
	in the TRIP data set	at the gauging station closest to the river mouth	
Mackenzie	1.74	1.66	Arctic red river
Yukon	0.85	0.83	Pilot Station
Columbia	0.66	0.64	See section 2.3
Fraser	0.23	0.22	Hope
Nelson	1.07	1.06	Long Spruce generating station
St. Lawrence	1.11	0.77	Cornwall, Ontario

382

383



384  
 385 **Figure 3:** Comparison of CanRCM4 simulated precipitation (left column) and temperature (right  
 386 column) with observation-based estimates from the CRU TS 4.07 data set for the period 1986-  
 387 2005.

388

### 389 3. Results

#### 390 3.1 Present-day precipitation, temperature, and streamflow

391 Figure 3 compares the geographical distribution of mean annual precipitation (left  
 392 column) and temperature (right column) simulated by CanRCM4 to observation-based estimates  
 393 from the CRU TS 4.07 data set (referred to as CRU from here on) for the 1986-2005 period.  
 394 Although the six river basins considered in this study do not cover the entire Canadian region, for

395 completeness the plots are shown for the whole of Canada and south up to 39 °N to include the  
396 southern edge of the Columbia River basin. In Figure 3, while CanRCM4 broadly simulates the  
397 geographical distribution of temperature and precipitation reasonably realistically, there are  
398 differences compared to the CRU data set. CanRCM4 generally simulates higher precipitation  
399 over Canada and more so to the west of the Rockies (Figure 3c) compared to observations. The  
400 model simulates cooler than observed temperatures to the west of the Rockies and higher than  
401 observed temperatures to the east of the Rockies (Figure 3f). This is likely related to the  
402 representation of topography in the model. The overall somewhat higher precipitation in  
403 CanRCM4 over North America is also noted by Alaya et al. (2019) who compared probable  
404 maximum precipitation (PMP) calculated using CanRCM4 data to estimates based on several  
405 reanalyses. Alaya et al. (2019) concluded that among the three reanalyses they considered,  
406 CanRCM4 compared best with the National Centre for Environmental Prediction's (NCEP) Climate  
407 Forecast System Reanalysis.

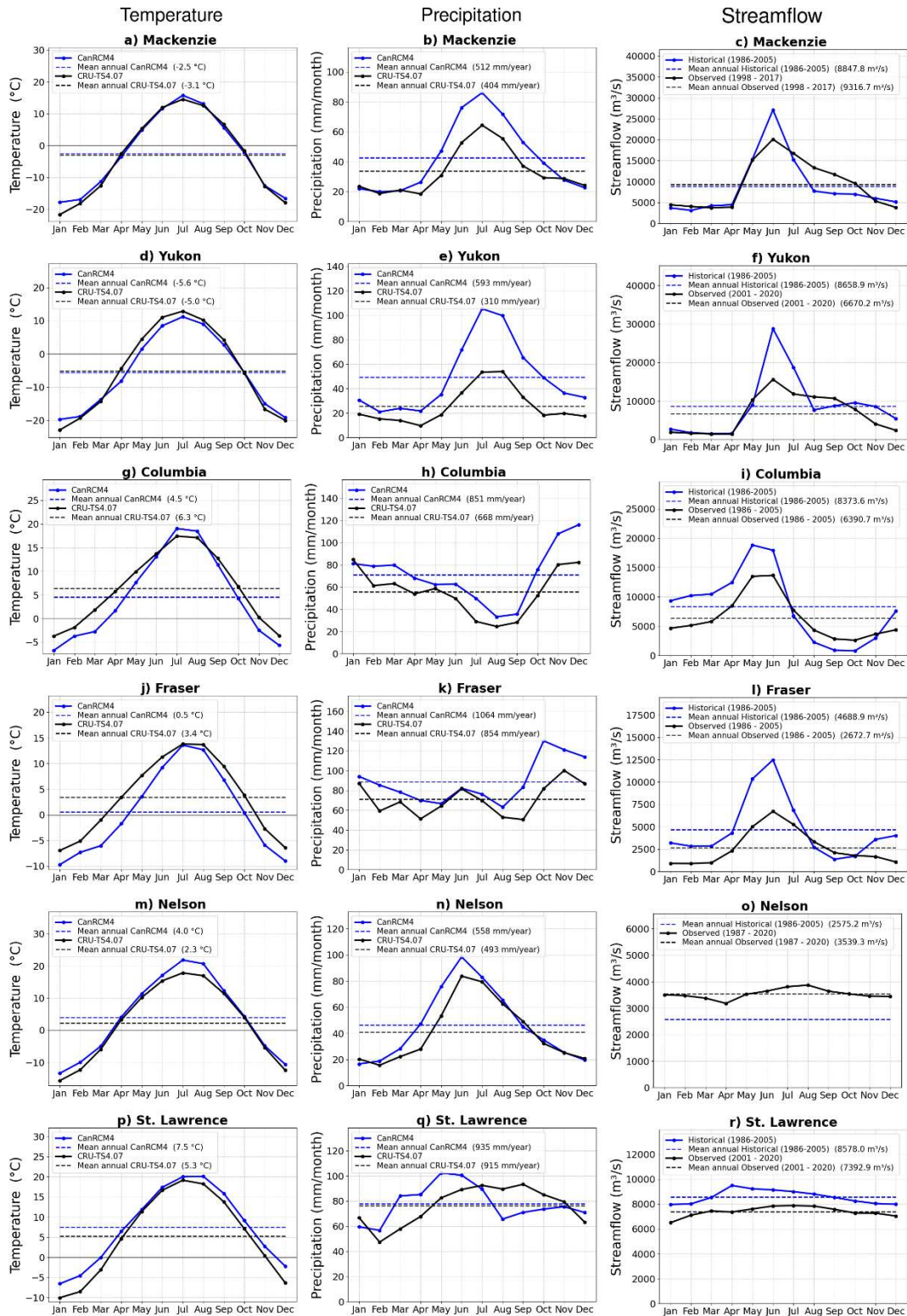
408 Figure 4 compares the simulated annual cycle of temperature (left column) and  
409 precipitation (middle column) over the six river basins (Figure 1) selected in this study with  
410 observation-based estimates from CRU. The right-hand side column compares simulated  
411 streamflow for the six river basins with observation-based estimates from the GRDC. The basin-  
412 averaged values of temperature and precipitation are calculated by area weighting the values in  
413 the individual grid cells that lie inside a given river basin according to the TRIP data (Figure 1).  
414 The plots also show the mean annual values (dashed lines) on the plot and their magnitude in  
415 the legend. Figure 4 shows that overall CanRCM4 simulated basin-wide averaged temperatures  
416 compare reasonably well with observation-based estimates based on the CRU data for the

417 Mackenzie and the Yukon River basins. For the Columbia and Fraser, the simulated temperatures  
418 are lower for most months, and for the Nelson River basin, the CanRCM4 simulated temperatures  
419 are higher compared to the CRU data. The seasonal cycle of temperature compares well with the  
420 observation-based estimates from CRU data. Compared to temperature, there are larger  
421 differences in simulated CanRCM4 precipitation compared to the CRU data. Although CanRCM4  
422 simulates the seasonality of precipitation reasonably well compared to the CRU data, simulated  
423 precipitation is higher for all river basins, consistent with Figure 3c. The comparison with the CRU  
424 data provides useful insights into simulated quantities. Specifically, despite the difference in the  
425 magnitudes, CanRCM4 provides a reasonable representation of the seasonality of precipitation,  
426 for example, higher winter precipitation in the southern Fraser and Columbia basins, and higher  
427 summer precipitation in the northern Mackenzie and Yukon basins. However, all observation-  
428 based data sets (including CRU) have their limitations. Wong et al. (2017) compared several  
429 gridded observation-based precipitation data sets over Canada and found that they all have  
430 limitations and the data sets compared best with gauge-based precipitation data in summer,  
431 followed by autumn, spring, and winter in order of decreasing quality. Sun et al. (2018) compare  
432 global precipitation from 22 gauge-, satellite-, and reanalysis-based products, including CRU, and  
433 quantify the uncertainty in the different precipitation estimates over timescales ranging from  
434 daily to annual. Shi et al. (2017) evaluated the CRU precipitation over large regions of China and  
435 found that CRU underestimates precipitation in that region compared to rain gauge records.  
436 Furthermore, observation-based precipitation datasets also generally tend to underrepresent  
437 total precipitation in mountainous western Canada (where the Yukon, Mackenzie, Fraser, and  
438 Columbia River basins are located) due to low station density at high elevations (Werner et al.,

439 2019). In the end, the objective of the comparison of the simulated climate with CRU  
440 observations is to evaluate if the model climate is reasonably realistic for the present day. The  
441 assumption behind using direct output from climate models is that despite the biases in the  
442 simulated current climate it is possible to deduce meaningful information about the effect of  
443 climate change using the change in simulated quantities.

444





445  
 446 **Figure 4:** Comparison of the annual cycle of basin-wide averaged CanRCM4 simulated  
 447 temperature (left column) and precipitation (middle column) with observation-based estimates  
 448 from the CRU TS 4.07 data set for the period 1986-2005. The right-hand side column compares

449 simulated streamflow with observations from the GRDC. In the absence of the consideration of  
450 anthropogenic flow regulation for the Nelson River only its simulated mean annual streamflow  
451 value is evaluated.

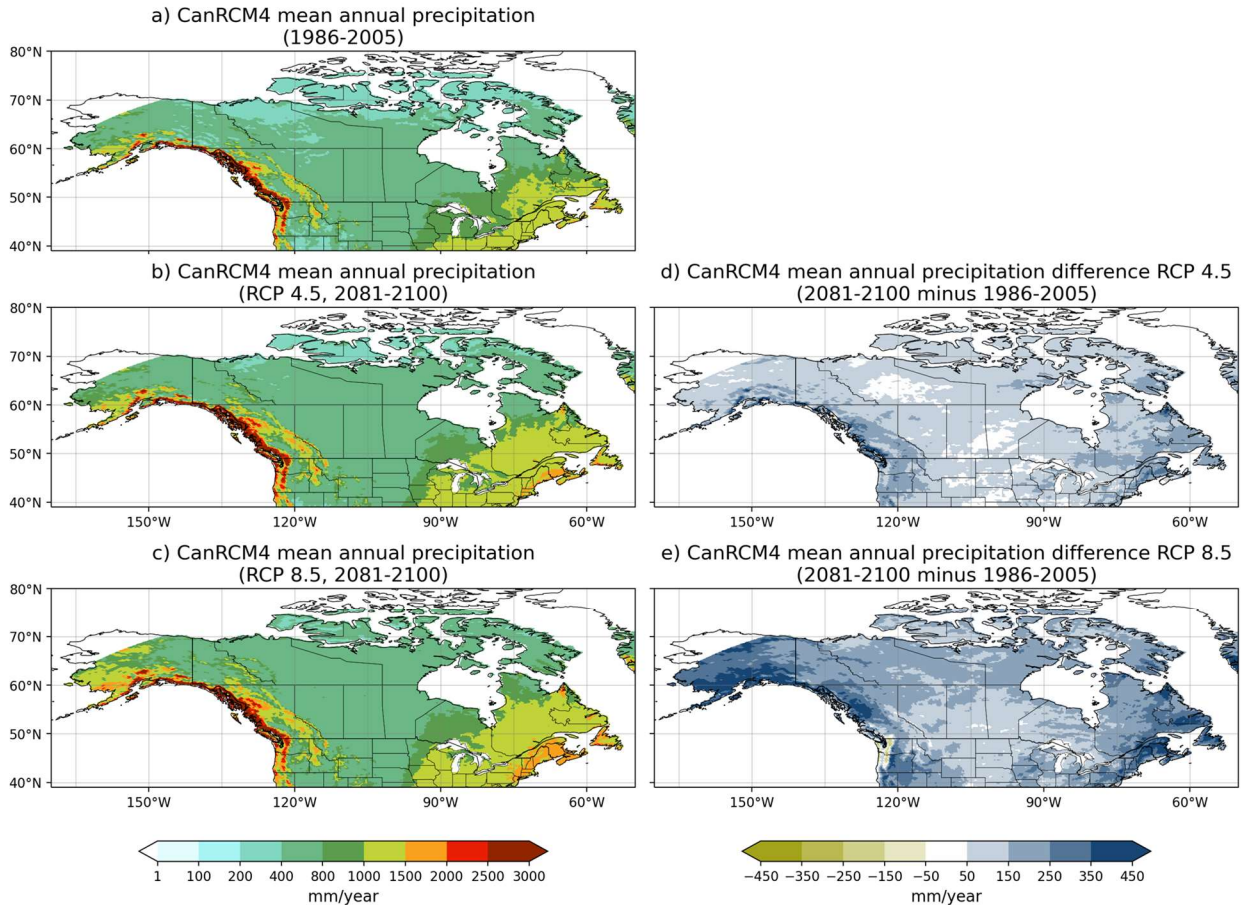
452

453         The differences in simulated climate between CanRCM4 and the observation-based  
454 climate in CRU for the present day affect simulated streamflow as expected. The simulated mean  
455 annual streamflow is higher for four out of six river basins considered (Yukon, Columbia, Fraser,  
456 and St. Lawrence) primarily because of the higher simulated precipitation. Simulated  
457 precipitation is also higher for the Mackenzie River basin, but the mean annual simulated  
458 streamflow compares well with its observation-based estimate. Possible reasons for reasonably  
459 realistic annual simulated streamflow despite higher precipitation could be biases in the CRU  
460 data set itself (e.g., underrepresentation of total annual precipitation), or higher simulated  
461 evaporation in CanRCM4 (although simulated summer temperatures compare well with the CRU  
462 data). Finally, the simulated mean annual streamflow for the Nelson River is lower than its  
463 observation-based estimate despite somewhat higher simulated precipitation than the CRU data.  
464 The most likely reason for this is the diversion from the Churchill River into the Nelson River which  
465 started in 1976 to increase the water flow to larger generating stations on the lower Nelson River.  
466 The Manitoba government estimates that an average of 25% more water flows into the lower  
467 Nelson River due to the Churchill River Diversion (CRD)  
468 (<https://www.gov.mb.ca/sd/water/water-power/churchill/index.html>, last accessed Sep. 2023).  
469 The seasonality of streamflow for the Mackenzie, Yukon, and Fraser Rivers is dominated by the  
470 spring snowmelt with the peak occurring in June for both simulated and observed streamflow.  
471 The simulated streamflow for the Columbia and Fraser rivers peaks at the right time but there is  
472 more simulated streamflow during the winter months when precipitation is also higher than

473 observed. For the Mackenzie and Yukon rivers although the mean annual simulated and observed  
474 streamflow are comparable their seasonal distribution is not. The simulated streamflow peak for  
475 these rivers is higher due to the simple treatment of ice jams which is not sufficient to hold the  
476 water in the river channel and then release it slowly as ice jams slowly dissipate in the spring and  
477 summer months, as the observed streamflow indicates. Finally, for the St. Lawrence River, there  
478 is little seasonality in observed streamflow due to the delay caused by the Great Lakes and  
479 anthropogenic flow regulation. The lack of strong seasonality simulated in simulated streamflow  
480 for the St. Lawrence River is caused entirely due to the delay caused by the Great Lakes (section  
481 2.2).

482 Overall the spatial distribution of precipitation and temperature over Canada (Figure 3),  
483 and the seasonality of these two primary climate drivers for the river basins considered in this  
484 study (Figure 4), compare reasonably well with observation-based estimates from the CRU data,  
485 although there are differences in the absolute magnitude of these variables. The resulting  
486 seasonality of streamflow has limitations due to three factors: 1) the biases in the driving climate  
487 from CanRCM4, 2) the biases in the land surface component of CanRCM4 which partitions  
488 precipitation into evaporation and runoff, 3) the lack of calibration of the land surface component  
489 to specific river basins, and 4) the lack of processes in the routing component including the  
490 limitation of not being able to treat ice jams comprehensively. Despite these limitations, the  
491 simulated streamflow captures the broad seasonal patterns with higher values during the spring  
492 snow melt and lower values during the winter months as observations show.

493



494 **Figure 5:** Comparison of CanRCM4 simulated precipitation for the 1986-2005 and for the 2081-  
 495 2100 periods for RCP 4.5 and 8.5 scenarios.

496

### 497 3.2 Changes in future climate and streamflow

498 Figures 5, 6, and 7 show the changes in CanRCM4 simulated precipitation, temperature,  
 499 and runoff for the period 2081-2100, for both RCP 4.5 and 8.5 scenarios, compared to the 1986-  
 500 2005 period from the historical simulation. Over Canada, simulated precipitation and  
 501 temperature increase almost everywhere and in both scenarios. As expected, the magnitude of  
 502 precipitation and temperature change is higher for the RCP 8.5 than the RCP 4.5 scenario.  
 503 Simulated precipitation increases are higher in the coastal western and eastern Canadian regions  
 504 than in central and northern parts of Canada. The central Canadian region sees the lowest

505 increase in precipitation in both scenarios. Simulated temperature increases, as expected, are  
506 higher at higher latitudes due to polar amplification of the temperature change associated with  
507 the snow- and ice-albedo feedbacks. In the RCP 4.5 and 8.5 scenarios, the simulated temperature  
508 changes vary from about 3 °C and 6 °C, respectively, in the south, to about 6 °C and 11 °C, in the  
509 north. The parent climate model (CanESM2) on which CanRCM4 is based has an equilibrium  
510 climate sensitivity of 3.7 °C, somewhat on the higher side, compared to the range of 1.5 °C to 4.5  
511 °C amongst climate models that contributed to CMIP5 (Schlund et al., 2020). As a result, we also  
512 expect the magnitude of simulated changes to be somewhat higher than a model with average  
513 climate sensitivity.

514

515

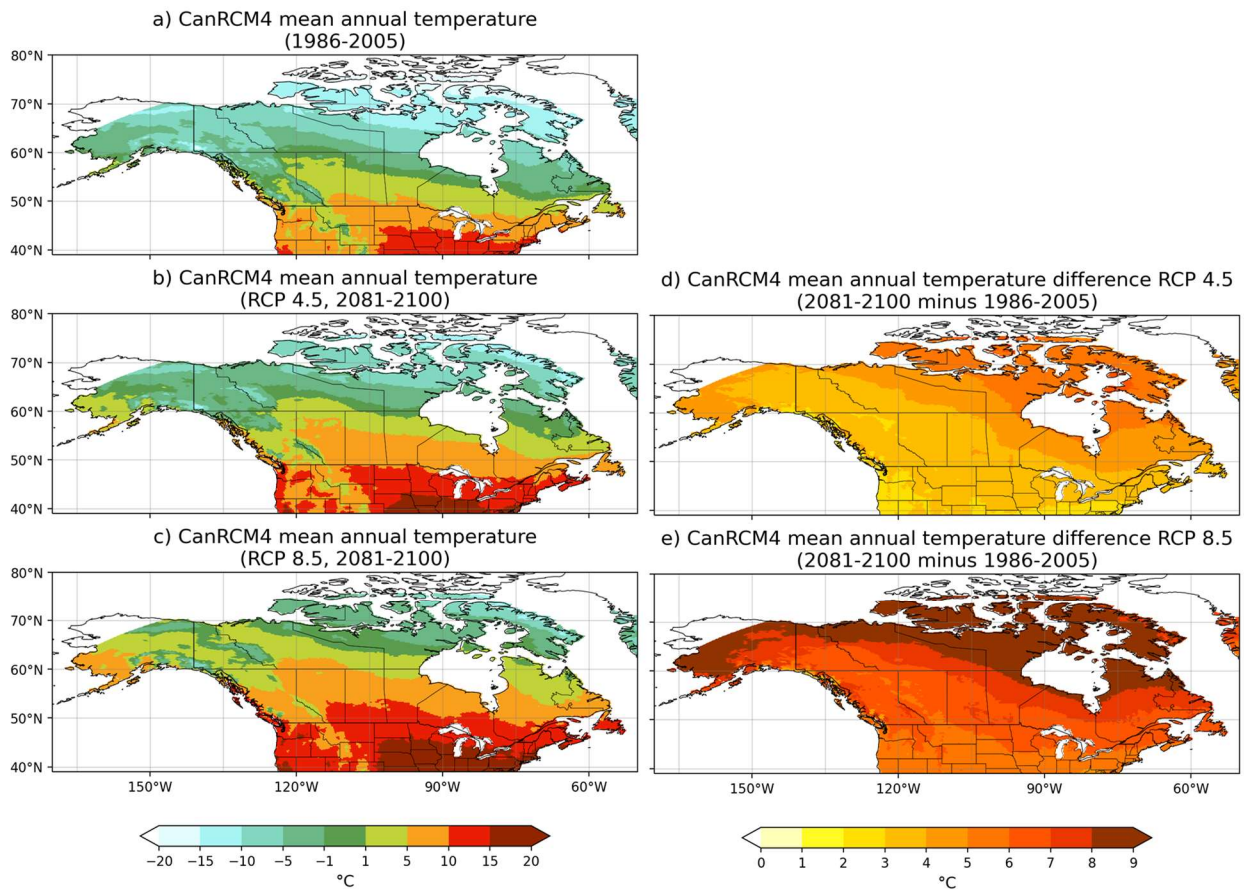
516

517

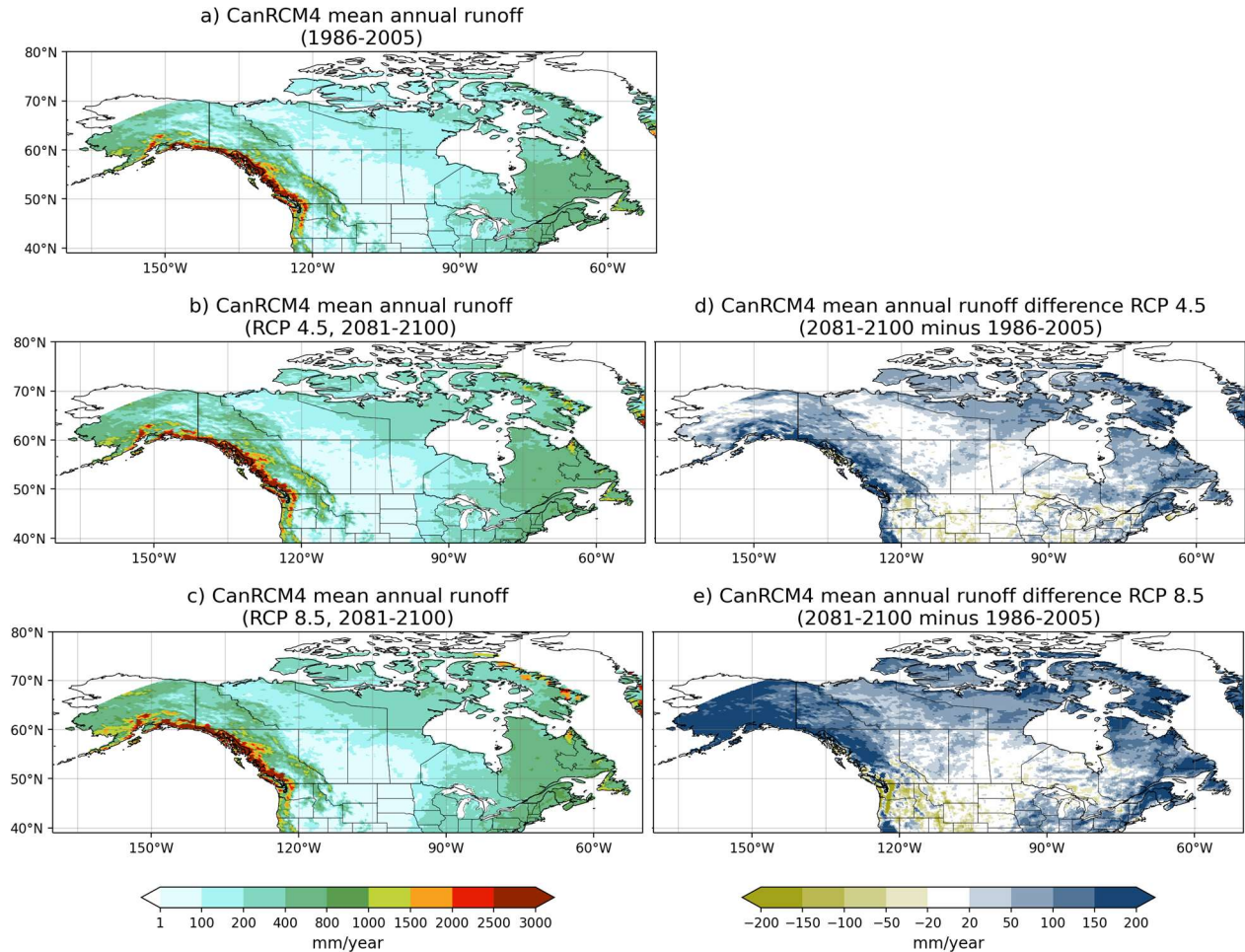
518

519

520



522 **Figure 6:** Comparison of CanRCM4 simulated temperature for the 1986-2005 period and for the  
523 2081-2100 periods, for RCP 4.5 and 8.5 scenarios.

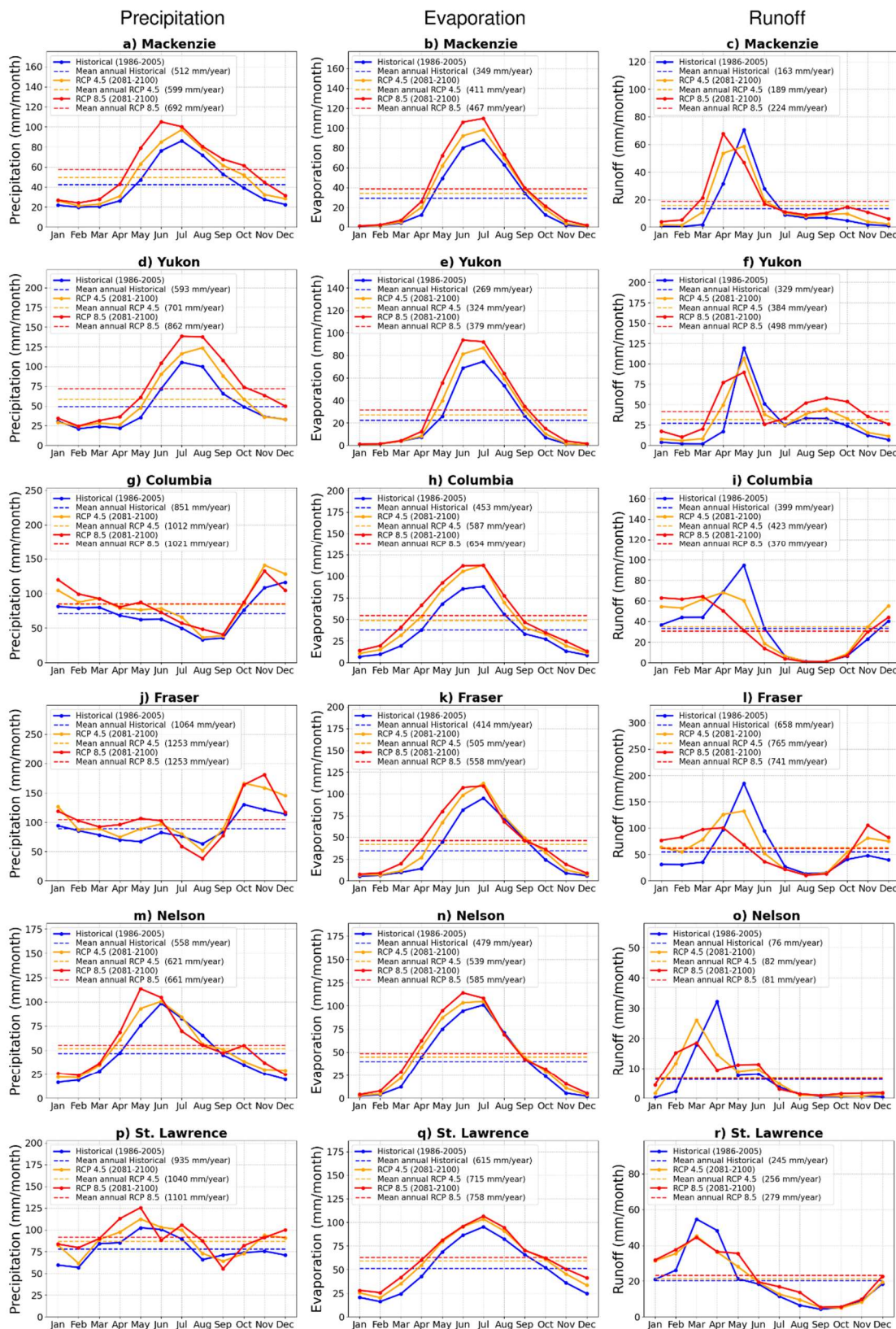


525

526 **Figure 7:** Comparison of CanRCM4 simulated runoff for the 1986-2005 period and the 2081-  
 527 2100 periods, for RCP 4.5 and 8.5 scenarios.

528

529 In Figure 7 runoff increases generally everywhere in Canada for the RCP 4.5 and RCP 8.5 scenarios  
 530 with larger changes on the west and east coasts, and in northern Canada, following a similar  
 531 pattern of changes in precipitation. Runoff reduces in parts of the southern Columbia River basin  
 532 in the United States in the RCP 4.5 scenario, and these decreases become more pronounced and  
 533 widespread over the north-western Pacific region in the RCP 8.5 scenario including the Fraser  
 534 River basin in Canada.



565 **Figure 8:** Comparison of the annual cycle of basin-wide averaged CanRCM4 simulated water  
 566 budget components for each river basin for the historical (1986-2005) period and the two future  
 567 scenarios RCP 4.5 and 8.5 (2081-2100): precipitation (left column), evaporation (middle column),  
 568 and runoff (right column).



569  
570  
571  
572  
573  
574  
575  
576  
577  
578  
579  
580  
581  
582  
583  
584  
585  
586  
587  
588  
589  
590  
591  
592  
593  
594  
595  
596  
597  
598  
599  
600  
601  
602  
603  
604  
605  
606  
607

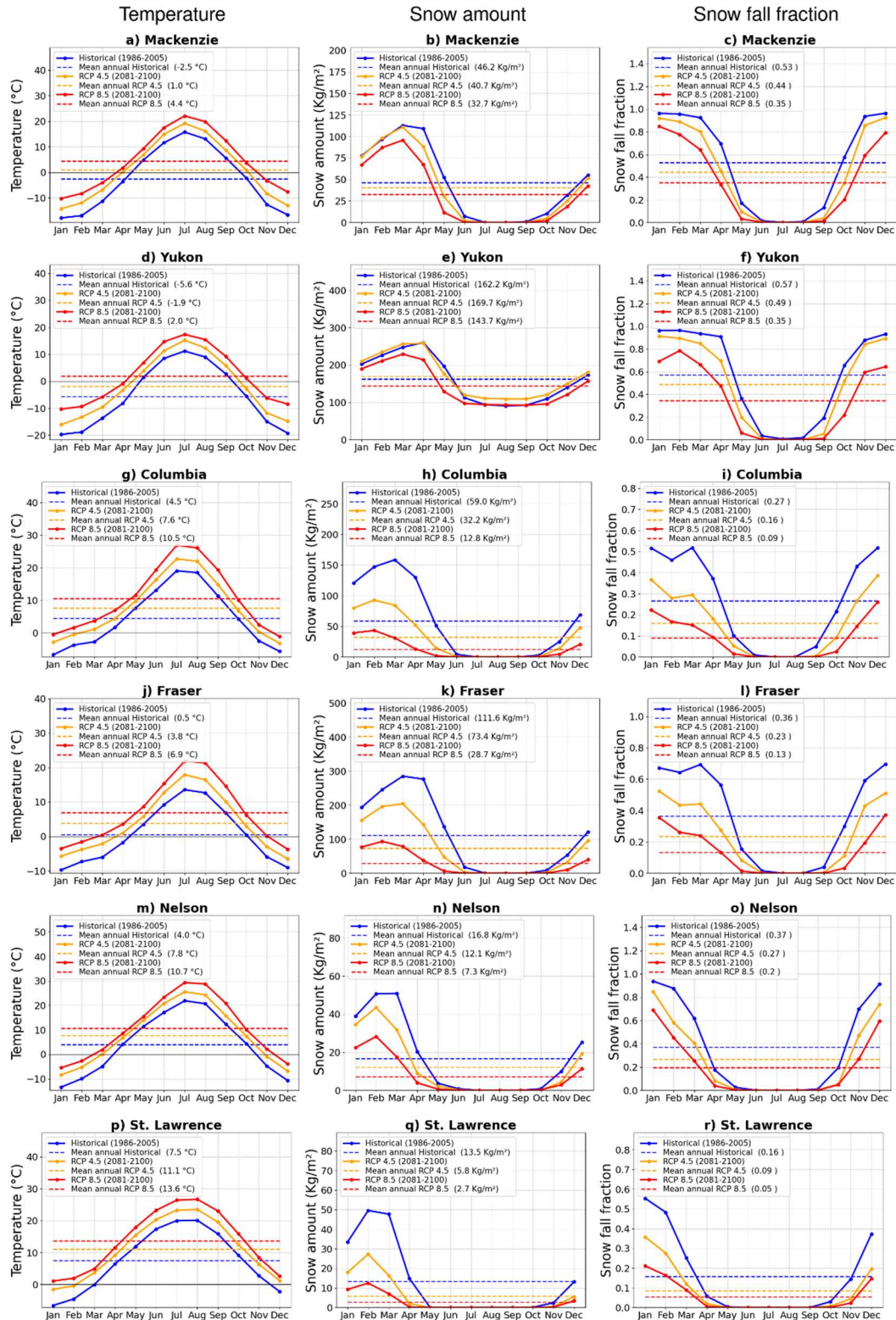


**Figure 9:** Comparison of the annual cycle of basin-wide averaged CanRCM4 simulated temperature (left column), snow water equivalent amount (middle column), and snowfall fraction (right column) for the historical (1986-2005) period and the two future scenarios RCP 4.5 and 8.5 (2081-2100).

612 Figure 8 shows the annual cycle of the simulated water budget components  
 613 (precipitation, evaporation, and runoff) for the six river basins considered in this study for the  
 614 historical (1986-2005) period and the two future scenarios, RCP 4.5 and 8.5 (2081-2100). As in  
 615 Figure 4, the mean annual values are shown as dashed lines, and their magnitude is noted in the  
 616 legend.

617 **Table 2:** Evaporation and runoff ratios for the six river basins simulated by CanRCM4 for the  
 618 historical period (1986-2005) and the two future scenarios (RCP 4.5 and 8.5, 2081-2100). The  
 619 evaporation (runoff) ratio is the ratio of mean annual evaporation (runoff) to precipitation.  
 620

River basin	Evaporation ratio (E/P)			Runoff ratio (R/P)		
	Historical (1986-2005)	RCP 4.5 (2081-2100)	RCP 8.5 (2081-2100)	Historical (1986-2005)	RCP 4.5 (2081-2100)	RCP 8.5 (2081-2100)
Mackenzie	0.682	0.686	0.675	0.318	0.316	0.324
Yukon	0.454	0.462	0.440	0.555	0.548	0.579
Columbia	0.532	0.580	0.641	0.469	0.418	0.362
Fraser	0.389	0.403	0.445	0.618	0.611	0.591
Nelson	0.858	0.868	0.885	0.136	0.132	0.123
St. Lawrence	0.664	0.686	0.684	0.314	0.294	0.302

621  
 622 The evaporation (E/P) and runoff (R/P) ratios for the six river basins for the historical period and  
 623 the two future scenarios are shown in Table 2 and allow to see how the partitioning of  
 624 precipitation into evaporation and runoff changes with climate. For the mean annual values of P,  
 625 E, and R reported in Figure 8, P is balanced to within 1% by E+R for all river basins (except St.  
 626 Lawrence) and all scenarios, except for the Yukon (for RCP 8.5) and Fraser River basins (for RCP  
 627 4.5 and 8.5) for which (E+R) is higher than P indicating that  $\Delta S$  is not zero (see equation 1). As a  
 628 result, (E/P) and (R/P) also add to one for all river basins except for the Yukon (RCP  
 629 8.5,  $(E + R)/P = 1.02$ ) and the Fraser River (RCP 4.5,  $(E + R)/P = 1.014$ , and RCP 8.5,  
 630  $(E + R)/P = 1.036$ ) basins. For the St. Lawrence River basin, the imbalance is around 2%  
 631 because of the presence of the Great Lakes which had to be excluded from the river basin mask.

632 Since basin-wide averaged calculations are done at 0.5° latitude-longitude resolution, and the  
633 actual domain of CanRCM4 is on a rotated latitude-longitude projection this led to slightly more  
634 rounding errors for the St. Lawrence than other river basins.

635 For all river basins considered, precipitation increases for both future scenarios with the  
636 increase being larger for the RCP 8.5 scenario consistent with Figures 5d and 5e. The response of  
637 evaporation to changes in climate is expected. The increase in precipitation and temperature  
638 yields an increase in evaporation for future scenarios for all river basins. Simulated runoff does  
639 not increase as much as precipitation since evaporation also increases. The runoff ratio, in Table  
640 2, increases for the northerly Mackenzie and the Yukon River basins while it decreases for the  
641 southerly Nelson, St. Lawrence, and especially for the Fraser and Columbia River basins which  
642 are characterized by milder climate owing to their location in the Pacific north-western region.  
643 This is because the increase in precipitation is more than enough to compensate for the increase  
644 in evaporation (associated with a warmer climate) for the northern river basins but not for the  
645 southern ones (as seen earlier in Figure 7 where runoff begins to decrease in parts of the  
646 Columbia and Fraser River basins). The absolute runoff amount in Figure 8 increases for the  
647 Mackenzie and Yukon River basins, in the RCP 4.5 and 8.5 scenarios compared to the historical  
648 simulation, but doesn't change much for the Columbia, Fraser, Nelson, and St. Lawrence River  
649 basins. However, the seasonality of runoff changes for all river basins, and the peak in simulated  
650 runoff either occurs earlier in the year, occurs with reduced magnitude, or both. Canadian rivers  
651 are dominated by spring snowmelt and this runoff behaviour is associated with snow melt  
652 occurring earlier in the year in the RCP 4.5 scenario than in the historical simulation and occurring  
653 even earlier in the RCP 8.5. This is seen in Figure 9 which shows the simulated annual cycle of

654 temperature changes, snow amount, and snowfall as a fraction of total precipitation for the  
655 historical period and the two RCP scenarios for the six river basins. In Figure 9 the mean annual  
656 temperature increases from the historical period to the RCP 4.5 scenario, and from the RCP 4.5  
657 to RCP 8.5 scenario, are between 3 and 3.5 °C for the six river basins considered here. The middle  
658 column of Figure 9 shows that in addition to earlier snowmelt the amount of snow in the winter  
659 months decreases for all river basins with climate warming. The only exception to this is the  
660 Yukon River basin in which the mean annual snow amount increases marginally in the RCP 4.5  
661 scenario (Figure 9e). As expected, the fraction of precipitation falling as snow also decreases with  
662 climate warming for all river basins (right column, Figure 9).

663

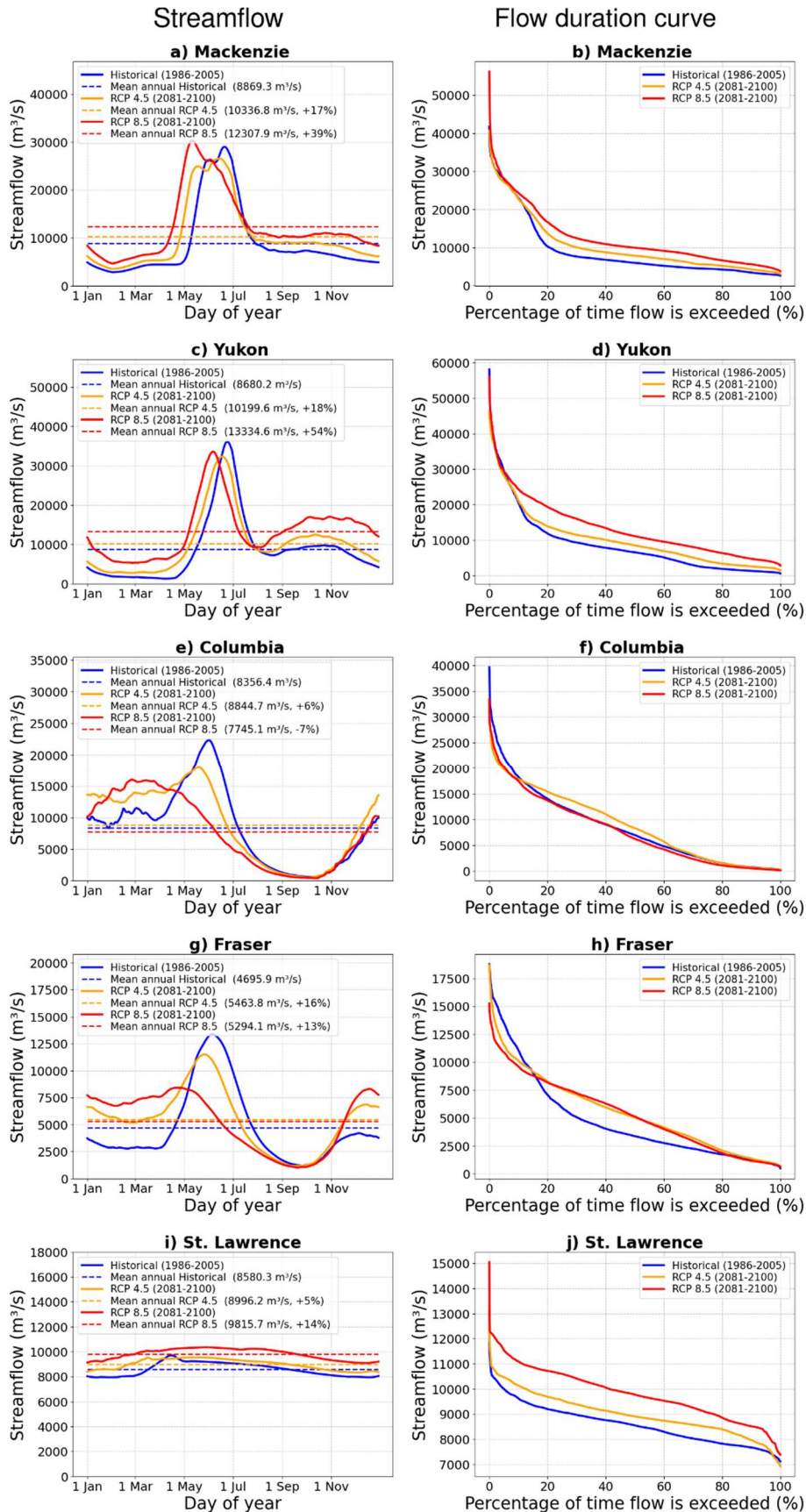
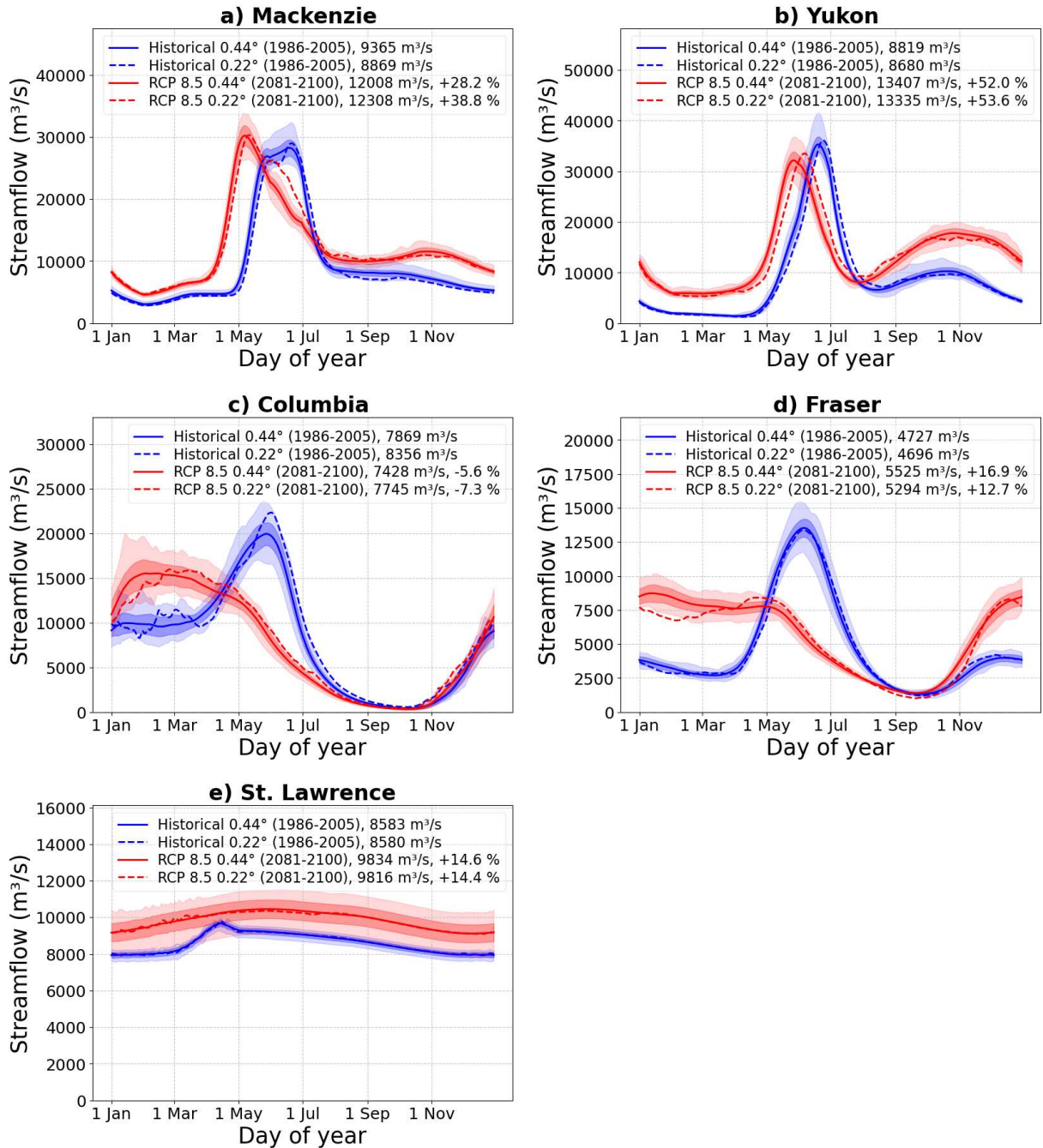


**Figure 10:** Comparison of the simulated daily streamflow (left column) and flow duration curves (right column) for the historical (1986-2005) period and the two future scenarios RCP 4.5 and 8.5 (2081-2100) for the river basins considered. The Nelson River is excluded for which we only evaluated annual streamflow values that are mentioned in the text.



690 **Figure 11:** Comparison of the simulated daily streamflow for the historical (1986-2005) period  
 691 and the RCP 8.5 scenario (2081-2100) for the river basins considered in this study from the  
 692 0.22° and 0.44° simulations. The results from the 0.22° simulations (shown earlier in Figure 10)  
 693 are shown as dashed lines. The uncertainty range for the 0.44° simulations is based on results  
 694 from CanRCM4's 50-member large ensemble. The solid lines indicate the mean across 50  
 695 members the light shading indicates the full range, and the dark shading indicates the mean ±  
 696 one standard deviation range, for the 0.44° simulations. The Nelson River is excluded for which

697 only annual streamflow values are analyzed.

698

699 Figure 10 compares simulated daily streamflow and flow duration curves averaged over  
700 the historical (1986-2005) period with those averaged over the two future scenarios RCP 4.5 and  
701 8.5 (2081-2100) for the river basins considered here excluding the Nelson River. The flow  
702 duration curves are calculated using daily streamflow values. The legends in Figure 10 for the  
703 streamflow figures in the left column show mean annual values but also the change from the  
704 simulated historical values for the RCP 4.5 and 8.5 scenarios. The mean annual streamflow  
705 increases for all rivers for both the RCP 4.5 and 8.5 scenarios, except for the Columbia River for  
706 the RCP 8.5 scenario (-7%). The increase in simulated annual streamflow is largest for the  
707 Mackenzie (+16%, +39%) and Yukon Rivers (+17%, +53%) for the RCP 4.5 and 8.5 scenarios, due  
708 to higher precipitation increase in these two basins (Figure 8). The increase in annual streamflow  
709 for other rivers is smaller and between 6% and 14%. Daily streamflow and flow duration curves  
710 are not shown for the Nelson River because we do not consider anthropogenic flow regulation,  
711 as mentioned earlier. The simulated mean annual streamflow for the Nelson River increases from  
712 2556.6 m<sup>3</sup>/s (for the 1986-2005 period) to 2774.8 and 2723.8 m<sup>3</sup>/s for the RCP 4.5 (+9%) and 8.5  
713 (+7%) scenarios, respectively (for the period 2081-2100).

714 The changes in streamflow seasonality are larger for the southerly Columbia and Fraser  
715 Rivers than for the northerly Mackenzie and Yukon Rivers. The peak daily streamflow for the  
716 Yukon River still occurs in June given it's the coldest river basin (Figure 4d) and the streamflow  
717 seasonality is still dominated by the spring snowmelt. The simulated daily peak streamflow for  
718 the Yukon River occurs on 24 June for the historical period (1986-2005), and 18 June and 6 June,

719 respectively, for RCP 4.5 and 8.5 scenarios for the period 2081-2100. Streamflow for the Yukon  
720 River also begins to increase earlier due to earlier snowmelt (Figure 9e). While the spring peak  
721 streamflow reduces in both RCP 4.5 and 8.5 scenarios during June and part of July, streamflow  
722 increases for most other months for the Yukon River. The Mackenzie River shows similar  
723 behaviour to the Yukon River in terms of earlier shifts of spring streamflow peaks with climate  
724 warming but the spring peak is higher for the RCP 8.5 scenario. The mean simulated daily peak  
725 streamflow for the Mackenzie River occurs on 21 June for the historical period (1986-2005), and  
726 14 June and 11 May, respectively, for RCP 4.5 and 8.5 scenarios for the period 2081-2100. Similar  
727 to Yukon, although the streamflow is lower for the Mackenzie River during June and part of July,  
728 it increases for most other months. The corresponding changes in streamflow are also seen in  
729 the flow duration curves. For these two rivers the frequency of the occurrence of flows that occur  
730 greater than about 5% of the time in the historical simulation increases in the future. The  
731 Columbia and the Fraser Rivers experience much larger changes in their seasonality as their  
732 primarily snow-dominated flow regimes change to more hybrid flow regimes. The snowmelt-  
733 driven streamflow peak in spring is reduced considerably for future scenarios since a lower  
734 fraction of fall, winter, and spring precipitation falls as snow. As a result, streamflow increases  
735 from October to April since precipitation falling as rain, as opposed to snow, yields runoff that  
736 runs straight into the rivers. Additionally, the large reduction in snowpack volume together with  
737 earlier melt (Figure 9k and 9h) affects the seasonality of the Fraser and Columbia Rivers  
738 streamflow and causes pronounced shifts in peak flows. The mean simulated daily peak  
739 streamflow for the Columbia River occurs on 1 June for the historical period (1986-2005), and 19  
740 May and 25 February, respectively, for RCP 4.5 and 8.5 scenario for the period 2081-2100. For



741 the Fraser River, the mean simulated peak streamflow occurs on 5 June for the historical period  
742 (1986-2005), and 26 May and 21 April, respectively, for RCP 4.5 and 8.5 scenario for the period  
743 2081-2100. The pronounced changes in the Fraser River basin peak flow are apparent in its flow  
744 duration curve (Figure 10h) which shows a decrease (increase) in the frequency of streamflow  
745 events which occurred less (more) than about 16% of the time and result in a more equitable  
746 streamflow regime with a pronounced reduction in its seasonality. The simulated streamflow for  
747 the St. Lawrence River shows very little seasonality and since annual streamflow increases for  
748 both scenarios, the flow duration curve simply moves up (Figure 10j).

### 749 **3.3 Uncertainty in simulated changes in future streamflow**

750 Using the large ensemble simulations that are available for the historical period and the  
751 RCP 8.5 scenario at 0.44 ° resolution we quantified the uncertainty in the simulated streamflow  
752 associated with the internal variability of the CanRCM4 model. Similar to the 0.22° resolution,  
753 we regridded the 0.44° runoff at CanRCM4's rotated latitude longitude projection to 0.5° regular  
754 latitude longitude projection for use as input into the river routing scheme. This is illustrated in  
755 Figure 11 which shows the simulated daily streamflow for all the rivers considered here except  
756 the Nelson River. In Figure 11, the solid lines show the average across the 50 members of the  
757 large ensemble, light shading shows the full range of the results, and dark shading shows the  
758 mean  $\pm$  one standard deviation range (this implies the 16%-84%, i.e. 68%, range when assuming  
759 normally distributed monthly streamflow values). In addition, streamflow from the 0.22°  
760 simulations (from Figure 10) is shown as dashed lines to allow direct comparison of results from  
761 the 0.22° and 0.44° simulations.

762 The changes in simulated streamflow are consistent between the 0.22° and 0.44°  
763 simulations. The results from the 0.44° simulations are also notably smoother compared to the  
764 0.22° simulations since the 0.44° results are also averaged over the 50 ensemble members in  
765 addition to the 20 years. For the most part, the results from the 0.22° simulations lie within the  
766 full range of results from the 0.44° simulations.  
767 This is expected since the driving climate at the boundaries of CanRCM4 based on CanESM2 is  
768 the same in both resolutions. The magnitude of change from the historical to the RCP 8.5 scenario  
769 (see legend for individual rivers) is, however, somewhat different. This is also expected because  
770 the coarser resolution 0.44° simulations are less representative of the basin topography than  
771 the 0.22° simulations. The day of peak streamflow occurs a few days earlier in 0.22° simulations  
772 than in the 0.44° simulations for the Mackenzie and Yukon Rivers. Overall, the large ensemble  
773 from the 0.44° simulations helps to provide context for results from the 0.22° simulations.

774 Overall, despite the differences in the magnitude of changes, the direction and variability  
775 of change obtained from this study is generally consistent with the previous studies using basin-  
776 scale hydrologic models, driven by statistically downscaled and bias-corrected climate model  
777 data, for instance for the Fraser River (Islam et al., 2019; Shrestha et al., 2012), the Columbia  
778 River (Schnorbus et al., 2014) and the Yukon River (Hay and McCabe, 2010). The results presented  
779 here are also comparable to the projections from global and regional scale hydrologic models,  
780 e.g. for the Mackenzie River basin (Krysanova et al., 2017, 2020).

#### 781 **4. Summary and conclusions**

782           This study offers a consistent analysis of results across six river basins in Canada based on  
783 results from the CanRCM4 model. Despite the biases in simulated present-day CanRCM4 climate,  
784 and some differences in the results based on 0.22° and 0.44° simulations, the results provide  
785 useful information about changes in simulated streamflow that is consistent with expectations  
786 of process behaviour in a warmer climate, and with published studies.

787           Neither future precipitation nor temperature changes are uniform across Canada.  
788 Simulated precipitation increases are higher closer to the west and east coasts, and simulated  
789 temperature changes are higher towards the Arctic. Similar to precipitation, runoff changes are  
790 also higher closer to the west and east coasts. The changes in simulated streamflow indicate how  
791 the present-day climate state of river basins plays a role in their response to climate change. The  
792 results yield two broadly distinct responses of monthly streamflow changes to climate warming,  
793 up until the end of this century, for the northerly Mackenzie and Yukon rivers and the southerly  
794 Fraser and Columbia rivers. Despite higher future projected temperature changes in Canada's  
795 north, peak streamflow for the Mackenzie and Yukon rivers is still dominated by the spring  
796 snowmelt. This is because the present-day colder states of these river basins imply that even  
797 after around 6-7 °C warming, the basin-wide average temperatures are cold enough to not  
798 sufficiently change their snowmelt-dominated streamflow regimes. Changes, however, do occur  
799 in streamflow seasonality for these two rivers. Mean peak daily streamflow occurs earlier by  
800 about 6-7 days for the Mackenzie and Yukon Rivers in the RCP 4.5 scenario and about 28 days for  
801 the Mackenzie River and 12 days for the Yukon River for the RCP 8.5 scenario (Figure 10). The  
802 earlier start of the snowmelt is the primary factor for the changes in peak streamflow and its time  
803 of occurrence, while the streamflow increases during the rest of the year (except for June and

804 part of July) are driven by an increase in precipitation. Additionally, a higher fraction of winter  
805 precipitation occurring as rainfall drives the winter streamflow increases. In contrast, the  
806 streamflow seasonality for the southerly Fraser and Columbia rivers is significantly more affected  
807 by warmer temperatures because the mean annual basin-wide temperature for these river basins  
808 is already above 0° C for the historical period. Both these rivers experience pronounced changes  
809 in their streamflow seasonality. The peak daily streamflow for both rivers decreases considerably  
810 and occurs about 45 days earlier for the Fraser River and about 100 days earlier for the Columbia  
811 River in the RCP 8.5 scenario. These results compare reasonably to the 1-2 months earlier peak  
812 in previous studies for the Fraser River (Islam et al., 2019; Shrestha et al., 2012) but are higher  
813 than the two months earlier peak for the Columbia River (Schnorbus et al., 2014) that used results  
814 from multiple climate models. Shrestha et al. (2021a) used CanRCM4 data to evaluate snowpack  
815 response to varying degrees of warming. They found that snowpack reduction using CanRCM4-  
816 LE is higher than the ensemble of results obtained by driving a hydrological model with data from  
817 other climate models (their supplementary information), consistent with CanESM2's higher  
818 climate sensitivity. For the Nelson and the St. Lawrence Rivers which show very little seasonality  
819 the effect of climate change is reflected in the changes in mean annual streamflow.

820         The results presented here also appear to show that the simulated changes in streamflow  
821 are somewhat resolution-dependent. This would be expected especially for topography-  
822 dominated river basins. If a large ensemble of 50 members for the 0.22° resolution was also  
823 available, it would have been easier to draw firm conclusions about the effect of the spatial  
824 resolution on changes in simulated streamflow.

825           There are two primary limitations of the work presented here. First, we use results from  
826 only one climate model. It would have been ideal to use runoff from other regional climate  
827 models to provide an uncertainty range based on the spread across different climate models.  
828 This would have also allowed us to evaluate how the spread across models compares to the  
829 spread across the 50 members of the CanRCM4 large ensemble. Second, the results are based on  
830 direct output from the CanRCM4 climate model and direct climate model output is biased. This  
831 limitation is tied to our methodology. The use of bias-corrected climate data inevitably implies  
832 using a different hydrological model or land surface scheme, than the land surface component of  
833 CanRCM4, and forcing it with bias-corrected climate data to obtain runoff. Finally, there are  
834 uncertainties associated with the routing process itself. As mentioned earlier, the routing scheme  
835 accounts for ice jams in a simplified manner, and anthropogenic flow regulation is not taken into  
836 account. The implicit assumption when using raw climate model output is that, despite the biases  
837 in simulated climate, it is possible to derive useful information about the impact of climate  
838 change on the simulated streamflow and other components of the hydrological budget. The  
839 Canada-wide results presented here have allowed us to differentiate between the hydrological  
840 response of the northerly Mackenzie and Yukon Rivers, and the southerly Fraser and Columbia  
841 Rivers, to climate change in a consistent manner. Furthermore, our results help fill the gaps in  
842 regions across Canada, where no climate model-driven hydrological projections are available.  
843 Within the scope of this study, we have only evaluated streamflow at the mouth of the six major  
844 rivers considered here. The full data set of daily simulated streamflow for the 20-year historical  
845 (1986-2005) and future periods (2081-2100) for the two scenarios, based on runoff from the  
846 0.22° simulations, is made available as detailed in the data availability section.

847 Large ensembles are now becoming more common. The challenge for similar future  
848 studies is to consider the inter-model and intra-model (based on ensemble members of the same  
849 model) spreads in the same framework to derive an uncertainty estimate that takes into account  
850 both types of uncertainties.

851  
852

### 853 **Acknowledgment**

854

855 We thank Daniel Peters for the helpful discussions at the beginning of this work and Sal Curasi  
856 and Gesa Meyer for providing comments on the final version of this manuscript. We also  
857 acknowledge the efforts of the climate modelling team at the Canadian Centre for Climate  
858 Modelling and Analysis (CCCma) who made the results from CanRCM4 available. We also thank  
859 the two anonymous reviewers who provided useful comments and helped us address the  
860 questions related to model bias and the differences in land surface and hydrological models.  
861 Finally, we would like to thank our handling editor (Alexander Gruber) for taking on our  
862 manuscript and giving us the opportunity to revise our manuscript.

863

### 864 **Data availability**

865

866 The CanRCM4 data from 0.22° simulations used in this study are available from CCCma website  
867 (<https://climate-modelling.canada.ca/climatemodeldata/canrcm/CanRCM4/>). The data from  
868 the 0.44° CanRCM4 large ensemble are available from Environment and Climate Change  
869 Canada (<https://open.canada.ca/data/en/dataset/83aa1b18-6616-405e-9bce-af7ef8c2031c>).

870

871 NetCDF files of simulated daily streamflow from the historical (1986-2005) and the two future  
872 scenarios (RCP 4.5 and 8.5, 2081-2100) at 0.5° resolution are available on Zenodo for the entire  
873 North American domain of CanRCM4 (doi:10.5281/zenodo.12775139,  
874 <https://zenodo.org/records/12775139>). These streamflow data correspond to the runoff from  
875 the 0.22° simulations.

876

### 877 **Author contributions**

878

879 VKA designed the study and wrote the majority of the manuscript. AL implemented river  
880 routing to operate at 0.5° resolution and performed all the simulations. RS and AL contributed  
881 to the manuscript text. RS also performed a literature review of existing studies that focus on

882 the impact of climate change on Canadian rivers.

883

#### 884 **Competing interests**

885

886 The authors declare that they have no competing interests.

887

#### 888 **References**

889 Alaya, M. A. B., Zwiers, F., and Zhang, X.: Evaluation and Comparison of CanRCM4 and CRCM5 to  
890 Estimate Probable Maximum Precipitation over North America, *J. Hydrometeorol.*, 20, 2069–2089,  
891 <https://doi.org/10.1175/JHM-D-18-0233.1>, 2019.

892 Arora, V., Seglenieks, F., Kouwen, N., and Soulis, E.: Scaling aspects of river flow routing, *Hydrol.*  
893 *Process.*, 15, 461–477, <https://doi.org/10.1002/hyp.161>, 2001.

894 Arora, V. K. and Boer, G. J.: Effects of simulated climate change on the hydrology of major river basins, *J.*  
895 *Geophys. Res. Atmospheres*, 106, 3335–3348, <https://doi.org/10.1029/2000JD900620>, 2001.

896 Arora, V. K. and Boer, G. J.: A Representation of Variable Root Distribution in Dynamic Vegetation  
897 Models, *Earth Interact.*, 7, 1–19, [https://doi.org/10.1175/1087-3562\(2003\)007<0001:AROVRD>2.0.CO;2](https://doi.org/10.1175/1087-3562(2003)007<0001:AROVRD>2.0.CO;2),  
898 2003.

899 Arora, V. K. and Boer, G. J.: A parameterization of leaf phenology for the terrestrial ecosystem  
900 component of climate models, *Glob. Change Biol.*, 11, 39–59, <https://doi.org/10.1111/j.1365-2486.2004.00890.x>, 2005.

902 Arora, V. K. and Boer, George. J.: A variable velocity flow routing algorithm for GCMs, *J. Geophys. Res.*  
903 *Atmospheres*, 104, 30965–30979, <https://doi.org/10.1029/1999JD900905>, 1999.

904 Arora, V. K. and Harrison, S.: Upscaling river networks for use in climate models, *Geophys. Res. Lett.*, 34,  
905 <https://doi.org/10.1029/2007GL031865>, 2007.

906 Arora, V. K., Boer, G. J., Christian, J. R., Curry, C. L., Denman, K. L., Zahariev, K., Flato, G. M., Scinocca, J.  
907 F., Merryfield, W. J., and Lee, W. G.: The Effect of Terrestrial Photosynthesis Down Regulation on the  
908 Twentieth-Century Carbon Budget Simulated with the CCCma Earth System Model, *J. Clim.*, 22, 6066–  
909 6088, <https://doi.org/10.1175/2009JCLI3037.1>, 2009.

910 Arora, V. K., Scinocca, J. F., Boer, G. J., Christian, J. R., Denman, K. L., Flato, G. M., Kharin, V. V., Lee, W.  
911 G., and Merryfield, W. J.: Carbon emission limits required to satisfy future representative concentration  
912 pathways of greenhouse gases, *Geophys. Res. Lett.*, 38, n/a-n/a,  
913 <https://doi.org/10.1029/2010GL046270>, 2011.

914 Beltaos, S.: Advances in river ice hydrology, *Hydrol. Process.*, 14, 1613–1625,  
915 [https://doi.org/10.1002/1099-1085\(20000630\)14:9<1613::AID-HYP73>3.0.CO;2-V](https://doi.org/10.1002/1099-1085(20000630)14:9<1613::AID-HYP73>3.0.CO;2-V), 2000.

916 Blyth, E. M., Arora, V. K., Clark, D. B., Dadson, S. J., De Kauwe, M. G., Lawrence, D. M., Melton, J. R.,  
917 Pongratz, J., Turton, R. H., Yoshimura, K., and Yuan, H.: Advances in Land Surface Modelling, *Curr. Clim.*  
918 *Change Rep.*, 2021.

919 Bolaños Chavarría, S., Werner, M., Salazar, J. F., and Betancur Vargas, T.: Benchmarking global  
920 hydrological and land surface models against GRACE in a medium-sized tropical basin, *Hydrol. Earth Syst.*  
921 *Sci.*, 26, 4323–4344, <https://doi.org/10.5194/hess-26-4323-2022>, 2022.

922 Bonsal, B., Shrestha, R. R., Dibike, Y., Peters, D. L., Spence, C., Mudryk, L., and Yang, D.: Western  
923 Canadian Freshwater Availability: Current and Future Vulnerabilities, *Environ. Rev.*, 28, 528–545,  
924 <https://doi.org/10.1139/er-2020-0040>, 2020.

925 Budhathoki, S., Rokaya, P., and Lindenschmidt, K.-E.: Impacts of future climate on the hydrology of a  
926 transboundary river basin in northeastern North America, *J. Hydrol.*, 605, 127317,  
927 <https://doi.org/10.1016/j.jhydrol.2021.127317>, 2022.

928 Chegwiddden, O. S., Nijssen, B., Rupp, D. E., Arnold, J. R., Clark, M. P., Hamman, J. J., Kao, S.-C., Mao, Y.,  
929 Mizukami, N., Mote, P. W., Pan, M., Pytlak, E., and Xiao, M.: How Do Modeling Decisions Affect the  
930 Spread Among Hydrologic Climate Change Projections? Exploring a Large Ensemble of Simulations  
931 Across a Diversity of Hydroclimates, *Earths Future*, 7, 623–637, <https://doi.org/10.1029/2018EF001047>,  
932 2019.

933 Chen, Y. and She, Y.: Long-term variations of river ice breakup timing across Canada and its response to  
934 climate change, *Cold Reg. Sci. Technol.*, 176, 103091,  
935 <https://doi.org/10.1016/j.coldregions.2020.103091>, 2020.

936 Côté, J., Gravel, S., Méthot, A., Patoine, A., Roch, M., and Staniforth, A.: The Operational CMC–MRB  
937 Global Environmental Multiscale (GEM) Model. Part I: Design Considerations and Formulation, *Mon.*  
938 *Weather Rev.*, 126, 1373–1395, [https://doi.org/10.1175/1520-0493\(1998\)126<1373:TOCMGE>2.0.CO;2](https://doi.org/10.1175/1520-0493(1998)126<1373:TOCMGE>2.0.CO;2),  
939 1998.

940 Deser, C., Lehner, F., Rodgers, K. B., Ault, T., Delworth, T. L., DiNezio, P. N., Fiore, A., Frankignoul, C.,  
941 Fyfe, J. C., Horton, D. E., Kay, J. E., Knutti, R., Lovenduski, N. S., Marotzke, J., McKinnon, K. A., Minobe, S.,  
942 Randerson, J., Screen, J. A., Simpson, I. R., and Ting, M.: Insights from Earth system model initial-  
943 condition large ensembles and future prospects, *Nat. Clim. Change*, 10, 277–286,  
944 <https://doi.org/10.1038/s41558-020-0731-2>, 2020.

945 Dibike, Y., Muhammad, A., Shrestha, R. R., Spence, C., Bonsal, B., de Rham, L., Rowley, J., Evenson, G.,  
946 and Stadnyk, T.: Application of dynamic contributing area for modelling the hydrologic response of the  
947 Assiniboine River basin to a changing climate, *J. Gt. Lakes Res.*, 47, 663–676,  
948 <https://doi.org/10.1016/j.jglr.2020.10.010>, 2021.

949 ECCC: The Canadian Regional Climate Model Large Ensemble. Environment and Climate Change Canada  
950 (ECCC), Government of Canada Open Data Portal. Available at:  
951 <https://open.canada.ca/data/en/dataset/83aa1b18-6616-405e-9bce-af7ef8c2031c>, Gatineau, QC,  
952 Canada, 2018.

953 Fisher, R. A. and Koven, C. D.: Perspectives on the Future of Land Surface Models and the Challenges of  
954 Representing Complex Terrestrial Systems, *J Adv Model Earth Syst*, 12, 2020.



- 955 Gosling, S. N., Taylor, R. G., Arnell, N. W., and Todd, M. C.: A comparative analysis of projected impacts  
956 of climate change on river runoff from global and catchment-scale hydrological models, *Hydrol. Earth*  
957 *Syst. Sci.*, 15, 279–294, <https://doi.org/10.5194/hess-15-279-2011>, 2011.
- 958 Harris, I., Osborn, T. J., Jones, P., and Lister, D.: Version 4 of the CRU TS monthly high-resolution gridded  
959 multivariate climate dataset, *Sci. Data*, 7, 109, <https://doi.org/10.1038/s41597-020-0453-3>, 2020.
- 960 Hattermann, F. F., Vetter, T., Breuer, L., Su, B., Daggupati, P., Donnelly, C., Fekete, B., Flörke, F., Gosling,  
961 S. N., P Hoffmann, Liersch, S., Masaki, Y., Motovilov, Y., Müller, C., Samaniego, L., Stacke, T., Wada, Y.,  
962 Yang, T., and Krysnova, V.: Sources of uncertainty in hydrological climate impact assessment: a cross-  
963 scale study, *Environ. Res. Lett.*, 13, 015006, <https://doi.org/10.1088/1748-9326/aa9938>, 2018.
- 964 Hay, L. E. and McCabe, G. J.: Hydrologic effects of climate change in the Yukon River Basin, *Clim. Change*,  
965 100, 509–523, <https://doi.org/10.1007/s10584-010-9805-x>, 2010.
- 966 Hewitson, B. C., Daron, J., Crane, R. G., Zermoglio, M. F., and Jack, C.: Interrogating empirical-statistical  
967 downscaling, *Clim. Change*, 122, 539–554, <https://doi.org/10.1007/s10584-013-1021-z>, 2014.
- 968 Huang, S., Shah, H., Naz, B. S., Shrestha, N., Mishra, V., Daggupati, P., Ghimire, U., and Vetter, T.: Impacts  
969 of hydrological model calibration on projected hydrological changes under climate change—a multi-  
970 model assessment in three large river basins, *Clim. Change*, 163, 1143–1164,  
971 <https://doi.org/10.1007/s10584-020-02872-6>, 2020.
- 972 Hundecha, Y., Arheimer, B., Berg, P., Capell, R., Musuuza, J., Pechlivanidis, I., and Photiadou, C.: Effect of  
973 model calibration strategy on climate projections of hydrological indicators at a continental scale, *Clim.*  
974 *Change*, 163, 1287–1306, <https://doi.org/10.1007/s10584-020-02874-4>, 2020.
- 975 Islam, S. U., Curry, C. L., Déry, S. J., and Zwiers, F. W.: Quantifying projected changes in runoff variability  
976 and flow regimes of the Fraser River Basin, British Columbia, *Hydrol. Earth Syst. Sci.*, 23, 811–828,  
977 <https://doi.org/10.5194/hess-23-811-2019>, 2019.
- 978 Ismail, H., Rowshon, M. K., Hin, L. S., Abdullah, A. F. B., and Nasidi, N. M.: Assessment of climate change  
979 impact on future streamflow at Bernam river basin Malaysia, *IOP Conf. Ser. Earth Environ. Sci.*, 540,  
980 012040, <https://doi.org/10.1088/1755-1315/540/1/012040>, 2020.
- 981 Kourzeneva, E., Asensio, H., Martin, E., and Faroux, S.: Global gridded dataset of lake coverage and lake  
982 depth for use in numerical weather prediction and climate modelling, *Tellus Dyn. Meteorol. Oceanogr.*,  
983 <https://doi.org/10.3402/tellusa.v64i0.15640>, 2012.
- 984 Krysnova, V., Vetter, T., Eisner, S., Huang, S., Pechlivanidis, I., Michael Strauch, Gelfan, A., Kumar, R.,  
985 Aich, V., Arheimer, B., Chamorro, A., Griensven, A. van, Kundu, D., Lobanova, A., Mishra, V., Plötner, S.,  
986 Reinhardt, J., Ousmane Seidou, Wang, X., Wortmann, M., Zeng, X., and Hattermann, F. F.:  
987 Intercomparison of regional-scale hydrological models and climate change impacts projected for 12  
988 large river basins worldwide—a synthesis, *Environ. Res. Lett.*, 12, 105002, <https://doi.org/10.1088/1748-9326/aa8359>, 2017.
- 990 Krysnova, V., Zaherpour, J., Didovets, I., Gosling, S. N., Gerten, D., Hanasaki, N., Müller Schmied, H.,  
991 Pokhrel, Y., Satoh, Y., Tang, Q., and Wada, Y.: How evaluation of global hydrological models can help to

- 992 improve credibility of river discharge projections under climate change, *Clim. Change*, 163, 1353–1377,  
 993 <https://doi.org/10.1007/s10584-020-02840-0>, 2020.
- 994 L. Sushama, R. Laprise, D. Caya, A. Frigon, and M. Slivitzky: Canadian RCM projected climate-change  
 995 signal and its sensitivity to model errors, *Int J Clim.*, 26, 2141–2159, 2006.
- 996 Lange, S.: Trend-preserving bias adjustment and statistical downscaling with ISIMIP3BASD (v1. 0),  
 997 *Geosci. Model Dev.*, 12, 2019.
- 998 MacDonald, M. K., Stadnyk, T. A., Déry, S. J., Braun, M., Gustafsson, D., Isberg, K., and Arheimer, B.:  
 999 Impacts of 1.5 and 2.0 °C Warming on Pan-Arctic River Discharge Into the Hudson Bay Complex Through  
 1000 2070, *Geophys. Res. Lett.*, 45, 7561–7570, <https://doi.org/10.1029/2018GL079147>, 2018.
- 1001 Manning, R.: On the flow of water in open channels and pipes, *Trans. Inst. Civ. Eng. Irel.*, XX, 161–207,  
 1002 1891.
- 1003 Maraun, D.: Bias Correcting Climate Change Simulations - a Critical Review, *Curr. Clim. Change Rep.*, 2,  
 1004 211–220, <https://doi.org/10.1007/s40641-016-0050-x>, 2016.
- 1005 Maraun, D., Shepherd, T. G., Widmann, M., Zappa, G., Walton, D., Gutiérrez, J. M., Hagemann, S.,  
 1006 Richter, I., Soares, P. M. M., Hall, A., and Mearns, L. O.: Towards process-informed bias correction of  
 1007 climate change simulations, *Nat. Clim. Change*, 7, 764–773, <https://doi.org/10.1038/nclimate3418>,  
 1008 2017.
- 1009 Miller, J. R. and Russell, G. L.: The impact of global warming on river runoff, *J. Geophys. Res.*  
 1010 *Atmospheres*, 97, 2757–2764, <https://doi.org/10.1029/91JD01700>, 1992.
- 1011 Miller, O. L., Putman, A. L., Alder, J., Miller, M., Jones, D. K., and Wise, D. R.: Changing climate drives  
 1012 future streamflow declines and challenges in meeting water demand across the southwestern United  
 1013 States, *J. Hydrol. X*, 11, 100074, <https://doi.org/10.1016/j.hydroa.2021.100074>, 2021.
- 1014 Moss, R. H., Edmonds, J. A., Hibbard, K. A., Manning, M. R., Rose, S. K., van Vuuren, D. P., Carter, T. R.,  
 1015 Emori, S., Kainuma, M., Kram, T., Meehl, G. A., Mitchell, J. F. B., Nakicenovic, N., Riahi, K., Smith, S. J.,  
 1016 Stouffer, R. J., Thomson, A. M., Weyant, J. P., and Wilbanks, T. J.: The next generation of scenarios for  
 1017 climate change research and assessment, *Nature*, 463, 747–756, <https://doi.org/10.1038/nature08823>,  
 1018 2010.
- 1019 Oki, T. and Sud, Y. C.: Design of Total Runoff Integrating Pathways (TRIP)—A Global River Channel  
 1020 Network, *Earth Interact.*, 2, 1–37, [https://doi.org/10.1175/1087-3562\(1998\)002<0001:DOTRIP>2.3.CO;2](https://doi.org/10.1175/1087-3562(1998)002<0001:DOTRIP>2.3.CO;2),  
 1021 1998.
- 1022 Overgaard, J., Rosbjerg, D., and Butts, M. B.: Land-surface modelling in hydrological perspective – a  
 1023 review, *Biogeosciences*, 3, 229–241, <https://doi.org/10.5194/bg-3-229-2006>, 2006.
- 1024 Poitras, V., Sushama, L., Seglenieks, F., Khaliq, M. N., and Soulis, E.: Projected Changes to Streamflow  
 1025 Characteristics over Western Canada as Simulated by the Canadian RCM, *J. Hydrometeorol.*, 12, 1395–  
 1026 1413, <https://doi.org/10.1175/JHM-D-10-05002.1>, 2011.

- 1027 Prowse, T. D.: Ice jam characteristics, Liard–Mackenzie rivers confluence, *Can. J. Civ. Eng.*, 13, 653–665,  
1028 <https://doi.org/10.1139/l86-100>, 1986.
- 1029 Quinn, F. H.: Hydraulic Residence Times for the Laurentian Great Lakes, *J. Gt. Lakes Res.*, 18, 22–28,  
1030 [https://doi.org/10.1016/S0380-1330\(92\)71271-4](https://doi.org/10.1016/S0380-1330(92)71271-4), 1992.
- 1031 Salathé, E. P., Leung, L. R., Qian, Y., and Zhang, Y.: Regional climate model projections for the State of  
1032 Washington, *Clim. Change*, 102, 51–75, <https://doi.org/10.1007/s10584-010-9849-y>, 2010.
- 1033 von Salzen, K., Scinocca, J. F., McFarlane, N. A., Li, J., Cole, J. N. S., Plummer, D., Versegny, D., Reader, M.  
1034 C., Ma, X., Lazare, M., and Solheim, L.: The Canadian Fourth Generation Atmospheric Global Climate  
1035 Model (CanAM4). Part I: Representation of Physical Processes, *Atmosphere-Ocean*, 51, 104–125,  
1036 <https://doi.org/10.1080/07055900.2012.755610>, 2013.
- 1037 Schlund, M., Lauer, A., Gentine, P., Sherwood, S. C., and Eyring, V.: Emergent constraints on equilibrium  
1038 climate sensitivity in CMIP5: do they hold for CMIP6?, *Earth Syst. Dyn.*, 11, 1233–1258,  
1039 <https://doi.org/10.5194/esd-11-1233-2020>, 2020.
- 1040 Schnorbus, M., Werner, A., and Bennett, K.: Impacts of climate change in three hydrologic regimes in  
1041 British Columbia, Canada, *Hydrol. Process.*, 28, 1170–1189, <https://doi.org/10.1002/hyp.9661>, 2014.
- 1042 Scinocca, J. F., Kharin, V. V., Jiao, Y., Qian, M. W., Lazare, M., Solheim, L., Flato, G. M., Biner, S.,  
1043 Desgagne, M., and Dugas, B.: Coordinated Global and Regional Climate Modeling, *J. Clim.*, 29, 17–35,  
1044 <https://doi.org/10.1175/JCLI-D-15-0161.1>, 2016.
- 1045 Shi, H., Li, T., and Wei, J.: Evaluation of the gridded CRU TS precipitation dataset with the point  
1046 raingauge records over the Three-River Headwaters Region, *J. Hydrol.*, 548, 322–332,  
1047 <https://doi.org/10.1016/j.jhydrol.2017.03.017>, 2017.
- 1048 Shrestha, R. R., Schnorbus, M. A., Werner, A. T., and Berland, A. J.: Modelling spatial and temporal  
1049 variability of hydrologic impacts of climate change in the Fraser River basin, British Columbia, Canada,  
1050 *Hydrol. Process.*, 26, 1840–1860, <https://doi.org/10.1002/hyp.9283>, 2012.
- 1051 Shrestha, R. R., Cannon, A. J., Schnorbus, M. A., and Alford, H.: Climatic Controls on Future Hydrologic  
1052 Changes in a Subarctic River Basin in Canada, *J. Hydrometeorol.*, 20, 1757–1778,  
1053 <https://doi.org/10.1175/JHM-D-18-0262.1>, 2019.
- 1054 Shrestha, R. R., Bonsal, B. R., Bonnyman, J. M., Cannon, A. J., and Najafi, M. R.: Heterogeneous snowpack  
1055 response and snow drought occurrence across river basins of northwestern North America under 1.0°C  
1056 to 4.0°C global warming, *Clim. Change*, 164, 40, <https://doi.org/10.1007/s10584-021-02968-7>, 2021a.
- 1057 Shrestha, R. R., Bonsal, B. R., Kayastha, A., Dibike, Y. B., and Spence, C.: Snowpack response in the  
1058 Assiniboine-Red River basin associated with projected global warming of 1.0 °C to 3.0 °C, *J. Gt. Lakes  
1059 Res.*, 47, 677–689, <https://doi.org/10.1016/j.jglr.2020.04.009>, 2021b.
- 1060 Sobie, S. R. and Murdock, T. Q.: Projections of Snow Water Equivalent Using a Process-Based Energy  
1061 Balance Snow Model in Southwestern British Columbia, *J. Appl. Meteorol. Climatol.*, 61, 77–95,  
1062 <https://doi.org/10.1175/JAMC-D-20-0260.1>, 2022.

- 1063 Stadnyk, T. A., Tefs, A., Broesky, M., Déry, S. J., Myers, P. G., Ridenour, N. A., Koenig, K., Vonderbank, L.,  
1064 and Gustafsson, D.: Changing freshwater contributions to the Arctic: A 90-year trend analysis (1981–  
1065 2070), *Elem. Sci. Anthr.*, 9, <https://doi.org/10.1525/elementa.2020.00098>, 2021.
- 1066 Sun, Q., Miao, C., Duan, Q., Ashouri, H., Sorooshian, S., and Hsu, K.-L.: A Review of Global Precipitation  
1067 Data Sets: Data Sources, Estimation, and Intercomparisons, *Rev. Geophys.*, 56, 79–107,  
1068 <https://doi.org/10.1002/2017RG000574>, 2018.
- 1069 Swart, N. C., Cole, J. N. S., Kharin, V. V., Lazare, M., Scinocca, J. F., Gillett, N. P., Anstey, J., Arora, V.,  
1070 Christian, J. R., Hanna, S., Jiao, Y., Lee, W. G., Majaess, F., Saenko, O. A., Seiler, C., Seinen, C., Shao, A.,  
1071 Sigmund, M., Solheim, L., von Salzen, K., Yang, D., and Winter, B.: The Canadian Earth System Model  
1072 version 5 (CanESM5.0.3), *Geosci. Model Dev.*, 12, 4823–4873, [https://doi.org/10.5194/gmd-12-4823-](https://doi.org/10.5194/gmd-12-4823-2019)  
1073 2019, 2019.
- 1074 Thrasher, B., Xiong, J., Wang, W., Melton, F., Michaelis, A., and Nemani, R.: Downscaled Climate  
1075 Projections Suitable for Resource Management, *Eos Trans. Am. Geophys. Union*, 94, 321–323,  
1076 <https://doi.org/10.1002/2013EO370002>, 2013.
- 1077 Trenberth, K. E., Smith, L., Qian, T., Dai, A., and Fasullo, J.: Estimates of the Global Water Budget and Its  
1078 Annual Cycle Using Observational and Model Data, *J. Hydrometeorol.*, 8, 758–769,  
1079 <https://doi.org/10.1175/JHM600.1>, 2007.
- 1080 Verseghy, D. L.: Class—A Canadian land surface scheme for GCMS. I. Soil model, *Int. J. Climatol.*, 11,  
1081 111–133, <https://doi.org/10.1002/joc.3370110202>, 1991.
- 1082 Verseghy, D. L., McFarlane, N. A., and Lazare, M.: Class—A Canadian land surface scheme for GCMS, II.  
1083 Vegetation model and coupled runs, *Int. J. Climatol.*, 13, 347–370,  
1084 <https://doi.org/10.1002/joc.3370130402>, 1993.
- 1085 Werner, A. T., Schnorbus, M. A., Shrestha, R. R., Cannon, A. J., Zwiers, F. W., Dayon, G., and Anslow, F.: A  
1086 long-term, temporally consistent, gridded daily meteorological dataset for northwestern North America,  
1087 *Sci. Data*, 6, 180299, <https://doi.org/10.1038/sdata.2018.299>, 2019.
- 1088 Winter, J. M. and Eltahir, E. A. B.: Modeling the hydroclimatology of the midwestern United States. Part  
1089 2: future climate, *Clim. Dyn.*, 38, 595–611, <https://doi.org/10.1007/s00382-011-1183-1>, 2012.
- 1090 Wong, J. S., Razavi, S., Bonsal, B. R., Wheeler, H. S., and Asong, Z. E.: Inter-comparison of daily  
1091 precipitation products for large-scale hydro-climatic applications over Canada, *Hydrol. Earth Syst. Sci.*,  
1092 21, 2163–2185, <https://doi.org/10.5194/hess-21-2163-2017>, 2017.
- 1093 Yoosefdoost, I., Khashei-Siuki, A., Tabari, H., and Mohammadrezapour, O.: Runoff Simulation Under  
1094 Future Climate Change Conditions: Performance Comparison of Data-Mining Algorithms and Conceptual  
1095 Models, *Water Resour. Manag.*, 36, 1191–1215, <https://doi.org/10.1007/s11269-022-03068-6>, 2022.
- 1096 Zhang, X., Tang, Q., Zhang, X., and Lettenmaier, D. P.: Runoff sensitivity to global mean temperature  
1097 change in the CMIP5 Models, *Geophys. Res. Lett.*, 41, 5492–5498,  
1098 <https://doi.org/10.1002/2014GL060382>, 2014.
- 1099

1100